Natural Resources Canada | Ressources naturelles Canada

GEOLOGICAL SURVEY OF CANADA
OPEN FILE 8337

Radiometric domains and the integration of multiple gamma-ray data sources for a remote area of northern Quebec

G. Hagedorn, R.C. Paulen, R. Fortin, and E. Arnaud

2018

Canada

GEOLOGICAL SURVEY OF CANADA
OPEN FILE 8337

Radiometric domains and the integration of multiple gamma-ray data sources for a remote area of northern Quebec

G. Hagedorn[1], R.C. Paulen[2], R. Fortin[2], and E. Arnaud[3]

[1]Department of Geography, 50 Stone Road East, University of Guelph, Guelph, Ontario N1G 2W1
[2]Geological Survey of Canada, 601 Booth Street, Ottawa, Ontario K1A 0E8
[3]School of Environmental Sciences, 50 Stone Road East, University of Guelph, Guelph, Ontario N1G 2W1

2018

© Her Majesty the Queen in Right of Canada, as represented by the Minister of Natural Resources, 2018

Information contained in this publication or product may be reproduced, in part or in whole, and by any means, for personal or public non-commercial purposes, without charge or further permission, unless otherwise specified.
You are asked to:

- exercise due diligence in ensuring the accuracy of the materials reproduced;
- indicate the complete title of the materials reproduced, and the name of the author organization; and
- indicate that the reproduction is a copy of an official work that is published by Natural Resources Canada (NRCan) and that the reproduction has not been produced in affiliation with, or with the endorsement of, NRCan.

Commercial reproduction and distribution is prohibited except with written permission from NRCan. For more information, contact NRCan at nrcan.copyrightdroitdauteur.rncan@canada.ca.

Permanent link: https://doi.org/10.4095/308209

This publication is available for free download through GEOSCAN (http://geoscan.nrcan.gc.ca/)

Recommended citation

Hagedorn, G., Paulen, R.C., Fortin, R., and Arnaud, E., 2018. Radiometric domains and the integration of multiple gamma-ray data sources for a remote area of northern Quebec; Geological Survey of Canada, Open File 8337, 1 .zip file. https://doi.org/10.4095/308209

Publications in this series have not been edited; they are released as submitted by the author.

TABLE OF CONTENTS

Introduction 1

Study site 2

Methods 5

Airborne gamma-ray spectrometry 5

Ground gamma-ray spectrometry 6

Laboratory gamma-ray spectrometry 7

Pebble lithologies 9

Data compilation 9

Results 9

Domain separation 9

Domain 1 10

Domain 2 11

Domain 3 13

Domain 4 13

Domain 5 13

Domain 6 13

Domain 7 13

Domain 8 13

Domain 9 13

Domain 10 13

Domain 11 14

Domain 12 14

Pebble counts 14

Comparison of gamma-ray spectrometry datasets 14

Discussion 15

Radiometric domain gamma-ray response 15

Comparison of gamma-ray spectrometry datasets 18

Implications for mineral exploration 18

Summary and conclusions 19

Acknowledgements 19

References 20

Appendices

Appendix A1. Site location information and results from field gamma-ray spectrometer measurements 22

Appendix A2. Site location information and results from laboratory gamma-ray spectrometer measurements 23

Figures

Figure 1. Schematic diagram illustrating the factors that can affect airborne gamma-ray survey measurements 2

Figure 2. Location map and detailed site map 3

Figure 3. Map of the bedrock geology in the study area 3

Figure 4. Digital elevation model of the study area 4

Figure 5. Map showing the directions of ice flow within the study area 5

Figure 6. Map of the study area shaded to reflect the relative surface concentrations of potassium, equivalent uranium, and equivalent thorium 6

Figure 7. Map showing the location where ground gamma-ray spectrometry measurements were taken 7
Figure 8. Photographs of a typical field station 8
Figure 9. Map of till sample location sites 8
Figure 10. Photographs of a sample tin and the laboratory gamma-ray spectrometer 9
Figure 11. Shaded map of the study area showing the interpreted radiometric domains 10
Figure 12. Map of the interpreted radiometric domains superimposed on a bedrock geology map of the study area 11
Figure 13. Photographs of pebble counts from samples collected 14
Figure 14. Scatterplot of gamma-ray responses measured in the field and in the laboratory versus the measurements from airborne spectrometry 15
Figure 15. Scatterplot of field measurements of potassium, equivalent uranium, and equivalent thorium in ground till versus bedrock 16
Figure 16. Scatterplot of potassium, equivalent uranium, and equivalent thorium measured in bedrock versus in till in the laboratory 16
Figure 17. Scatterplot of potassium, equivalent uranium, and equivalent thorium measured in ground till versus in the laboratory 17

Tables

Table 1. Domain average gamma-ray spectrometer measurements from airborne, bedrock, till in the field, and till in the laboratory 11
Table 2. General characteristics of the interpreted radiometric domains 12

Radiometric domains and the integration of multiple gamma-ray data sources for a remote area of northern Quebec

G. Hagedorn[1], R.C. Paulen[2], R. Fortin[2],and E. Arnaud[3]

[1]Department of Geography, University of Guelph, Guelph, Ontario N1G 2W1
[2]Geological Survey of Canada, 601 Booth Street, Ottawa, Ontario K1A 0E8
[3]School of Environmental Sciences, University of Guelph, Guelph, Ontario N1G 2W1

INTRODUCTION

Gamma radiation is high-frequency energy released by an unstable nucleus following radioactive decay. The main natural radioactive isotopes producing detectable gamma radiation within the Earth's crust are potassium-40, uranium-238, and thorium-232 (Minty, 1997). Concentrations of potassium, uranium, and thorium can therefore be inferred by measuring gamma-radiation intensities of earth materials.

Knowledge of the radioelement concentrations is useful in geology. Materials present at the Earth's surface (e.g. bedrock, glacial sediments, nonglacial sediments) have different gamma-ray signatures due to distinct concentrations of radioelements. For example, Gamma Ray Spectrometry (GRS) surveys can be used to map the extent of areas with distinct radio-chemical compositions that may coincide with surficial geological units. Another application of GRS is the mapping of dispersion trains in glacial sediments in which the bedrock sources have contrasting radioelement concentrations (Campbell et al. 2007; Ross et al., 2009; Fortin et al., 2015; Paulen et al., 2017). Dispersal trains of valuable mineralization in iron oxide – copper – gold, porphyry copper, and tin have been identified through the elevated potassium, uranium, and thorium levels associated with these deposits (Boyle, 1988; Ford et al., 2008).

GRS measurements can be obtained from airborne surveys, in-situ from handheld spectrometers, and from laboratory instruments. Each approach provides complementary but distinct information expressing a different scale of observation. Airborne GRS measurements are taken by flying over a desired area with a large-volume gamma-ray detector (International Atomic Energy Agency, 2003). This captures a combined signal of the upper 50 cm over a wide area. Airborne GRS spatial resolution is usually a few hundred of metres across. Ground GRS measurements can be obtained using handheld GRS instruments, and provide the average potassium, uranium, and thorium concentrations of a localized area within a few metres around the sensor. Ground measurements are used to target bulk till surfaces or bedrock outcrops. Finally, sediment samples can be collected and analyzed with a laboratory GRS instrument. Laboratory analysis provides the gamma-ray signature of solely the material itself, eliminating any outside gamma-ray sources.

Two environmental influences can affect field GRS measurements: cosmic and atmospheric radiation, and water, standing, interstitial, or contained in vegetation. Cosmic gamma-rays originating from extraterrestrial objects, including the sun, and atmospheric gamma-rays resulting from the decay of radon in the Earth's atmosphere can both influence airborne GRS measurements (Fig. 1) (Grasty et al., 1988; Gastrich et al., 2016). Cosmic and atmospheric radiation are corrected using standardized procedures (International Atomic Energy Agency, 2003). Water at surface or within the soil and vegetation also impacts GRS readings, absorbing gamma radiation and weakening the gamma-ray response (Fig. 1) (Gastrich et al., 2016). Consequently, areas of higher moisture content will have a fainter signature and lakes will absorb the signal completely (International Atomic Energy Agency, 2003). Water affects ground GRS measurements to a lesser extent than airborne measurements, as the sampled area can be targeted to flat and dry locations (International Atomic Energy Agency, 2003; Gastrich et al., 2016).

After obtaining a corrected radioelement concentration, airborne GRS data can then be analyzed by outlining radiometric domains. A radiometric domain is defined as an area of airborne response that is distinct from surrounding areas (Campbell et al., 2007; Fortin et al., 2015). Domains do not necessarily imply a homogeneous radioelement concentration but rather that the delineated area has internally consistent ratios of these radioelements that are distinct from the surrounding areas (Fortin et al., 2015). Radiometric domains are useful to locate anomalous GRS responses within a domain by comparing actual to expected radioelement compositions. Identification of these anomalous areas within a domain allows for more precise investigation into the cause of the anomalous signal, which is often geologically significant (Fortin et al., 2015). A useful application of this method is in mineral exploration, as gamma-ray anomalies can be the result of surficial areas with differing geochemistry, which could indicate a potential for mineralization (Campbell et al., 2007; Fortin et al., 2015). This method could also be useful in determining surficial

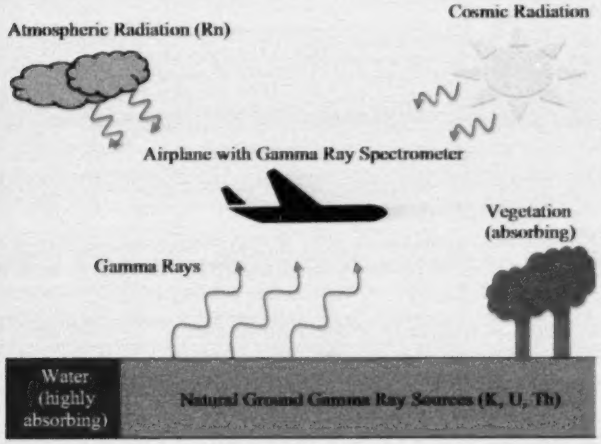

Figure 1. Many factors affect airborne gamma-ray survey measurements. Water and vegetation absorb the naturally released gamma rays from potassium, uranium, and thorium on the surface. In addition, other background influences can include cosmic radiation and atmospheric gamma-ray sources caused by the decay of radon.

geology as anomalies could be related to different sediment types.

Previous studies have looked at the association of ground and airborne measurements (Campbell et al., 2007; Fortin et al., 2015) but few have focused on the association and correlation among all three: airborne, ground in-situ, and laboratory GRS datasets. Any linkage in these values would be beneficial for mineral exploration. Geophysical surveys are quick and cost efficient, and consequently are often the first form of reconnaissance in an area (Kearey et al., 2013). Correlations could provide estimates for in situ values at a location, prompting discrimination of an anomalous signature and enabling more detailed identification of prospective locations.

The purpose of this research is to analyze different GRS datasets as part of a multidisciplinary collaborative research project with the Geological Survey of Canada to help guide mineral exploration in a remote region of northern Quebec (McClenaghan et al., 2016). First, radiometric domains will be qualitatively defined in the area based on airborne gamma-ray response. Second, the relationships among four different GRS datasets will be examined: airborne, in situ bedrock surface, in situ till surface, and laboratory analysis of till samples. This will exemplify the usefulness of radiometric domains in a geological context as well as describe connections among potassium (K), equivalent uranium (eU), and equivalent thorium (eTh) values from GRS of different spatial scales and sources. Understanding these two objectives can help to focus mineral exploration efforts by identifying potential targets and thereby reducing the amount of resources required to find valuable mineral deposits.

STUDY SITE

The study site in northern Quebec is approximately 100 km northeast of the community of Schefferville, in the Lac Résolution topographic map sheet (Fig. 2) (National Topographic System NTS 23P). The project was limited to the northwest portion of the Lac Résolution sheet (NTS 23P-11, -12, -13, and -14), where complete airborne GRS coverage was available, and ground sampling sites were taken at approximately 10 km intervals. The study area is in the Whale Lowland Region of the George Plateau in the Canadian Shield (Bostock, 1970). The topography is generally undulating moderate relief, with irregular glacially streamlined bedrock highs and lake-filled interlaying lows.

The region is centred on the Archean cratonic Meta Incognita rocks between the Torngat and the New Quebec orogenic rocks (Fig. 3) (Wardle and Bailey, 1981; Corrigan et al., 2009). The bedrock geology within this region is complex, of varying ages, and has been reworked by the collision of the Superior and the North Atlantic Cratons ca. 1.8 to 1.9 Ga (Sanborn-Barrie, 2016). The 1810–1837 Ma De Pas Batholith, which dominates the eastern side of the study area, is rimmed by orthogneiss and has potassium-rich rock with high zircon and light rare earth element chemistry (Fig. 3) (Sanborn-Barrie, 2016). Bedrock in the southeastern portion of the study area is dominated by the Churchill Province basement rocks and is overlain by Doublet Group fine-grained mafic metavolcanic rocks (amphibolite/metabasalt units) (Fig. 3). The Laporte Domain, found in the northwest portion, is characterized by different clastic metasedimentary rocks (greywacke, shale biotite schist, and quartzofeldspathic gneiss units) and typically contain no K-feldspar (Fig. 3) (Sanborn-Barrie, 2016). The De Pas Batholith is separated from the Doublet Group and Laporte Domain by a north–south oriented shear zone (Fig. 3) (Ministère de l'Énergie et des Ressources naturelles, 2010).

The topography within the study area varies east and west of the shear zone (Fig. 4). The eastern half is dominated by bedrock topographic highs, which reach 666 m above sea level (ASL) and are due to the De Pas Batholith's resistance to weathering (Fig. 4). The De Pas River channel has eroded through the eastern terrain, to the lowest elevation within the study area, at 307 m ASL (Fig. 4). West of the shear zone, the study area has relatively low topography (~450 m ASL) with little relief and contains the majority of lakes in the region. These characteristics relate to the underlying bedrock units, which are less resistant to weathering

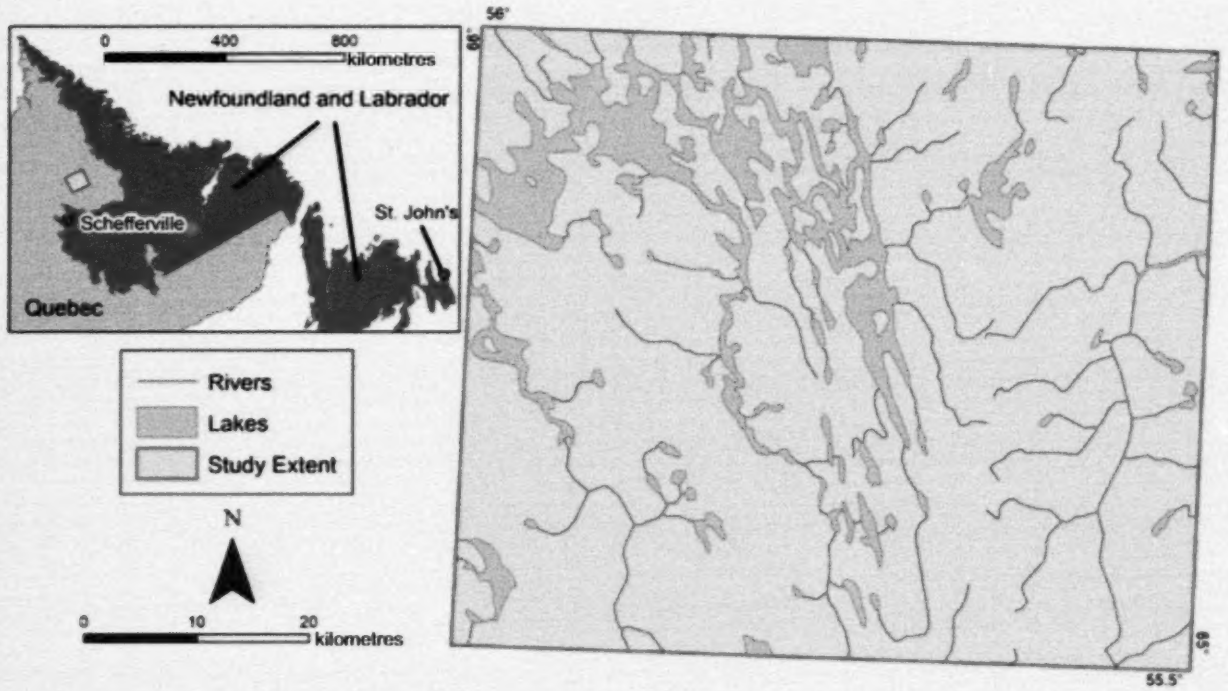

Figure 2. The study site is in northern Quebec, approximately 100 km northeast of the community of Schefferville, in the Lac Résolution topographic map sheet (NTS 23P), UTM Zone 20N.

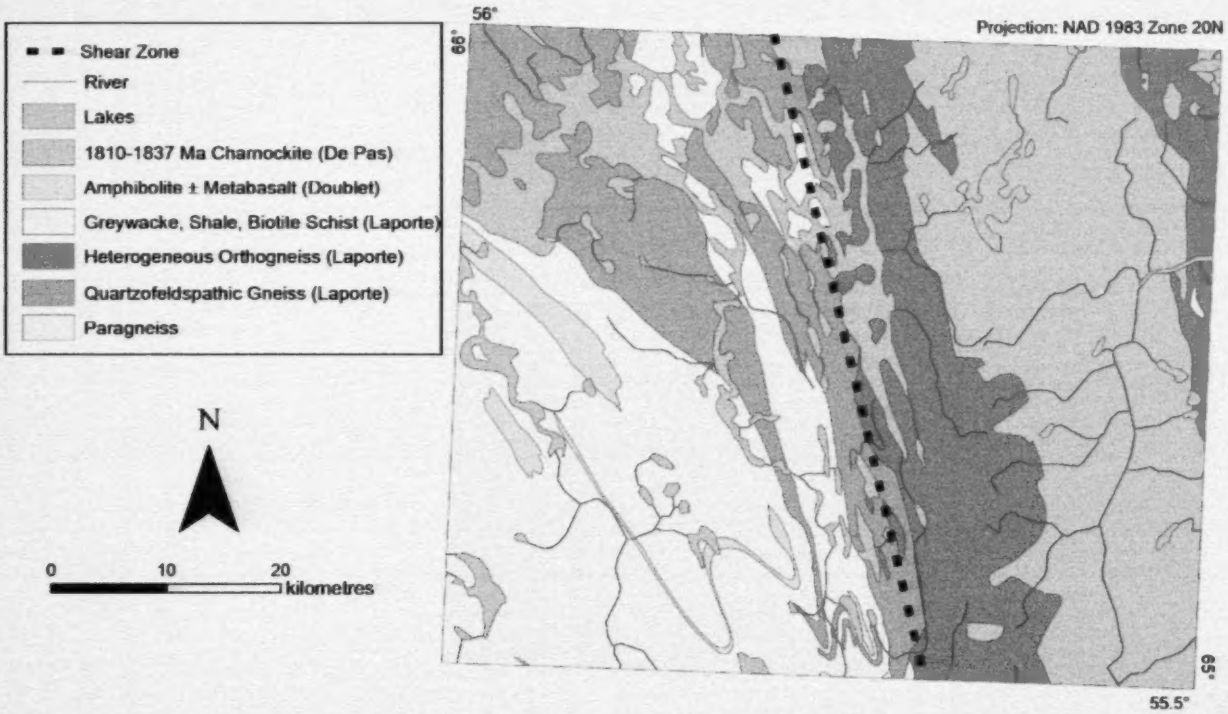

Figure 3. Map showing the bedrock geology in the study area (Sanborn-Barrie, 2016). The eastern portion is characterized by the De Pas Batholith rimmed by belts of orthogneiss. The western portion typically consists of metasedimentary units of the Laporte Domain.

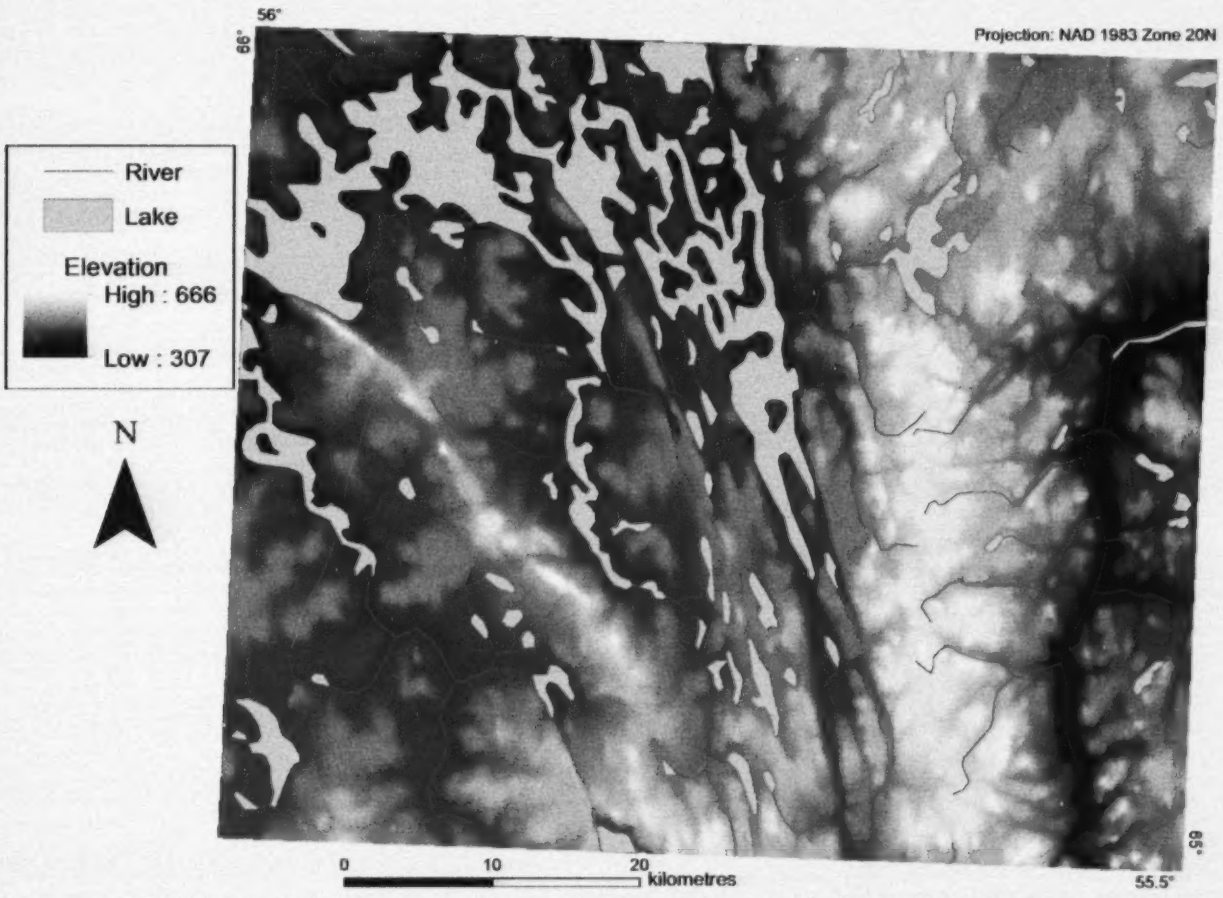

Figure 4. Digital elevation model (30 m x 30 m) of the study area from the Canadian Digital Elevation Data series (Canadian Centre for Mapping and Earth Observation, 1997). Relatively higher elevations occur in the eastern portion of the area and the lowest elevations occur along the De Pas River channel to the far east. The western portion of the study area has lower topography, which is associated with an increased number and size of lakes.

(Fig. 4). There is one northwest–southeast ridge in the western part of the study area with uncharacteristically high elevation, which is associated with quartzite of the Laporte Domain metasedimentary rocks.

The glacial history of the area is complex. Rice et al. (2016) found evidence that as many as four ice-flow phases impacted the region, with the oldest flow phase (pre-Wisconsin) to the northeast (Fig. 5) (Veillette et al., 1999). The second phase was radial flow out from the Ancestral Labrador ice divide east of the study area, which flowed westward across the De Pas Batholith (Fig. 5) (Vincent, 1989). The third phase was radial flow that occurred as the ice divide shifted to the west, causing ice movement to reverse and head eastward across the De Pas Batholith (Fig. 5). The final flow phases were associated with the deglaciation of the Laurentide Ice Sheet. In the eastern and southern portions of the map area, ice flow was eastward toward the ice margins in the Labrador Sea (Klassen and Thompson, 1993). In the southwest part of the study area, ice flow was to the southwest. In the northwest corner, ice flowed to the northwest, influenced by a large ice stream in the area (Fig. 5) (Jansson et al., 2003). The composition of the glacial sediment is directly related to the bedrock that the ice passes over, as it erodes and incorporates this bedrock material. Ice sheets also morph the landscape as they move through erosive and depositional forces. The net results of these multiple ice-flows are distinct till compositions and complex landforms.

The study area is characterized by thick continuous subglacial till blankets (>2 m) in the topographic lows and patchy subglacial till veneers (<2 m) and associated bedrock outcrops with mudboils on the topographic highs (McClenaghan et al., 2016; Rice et al., 2017). Low-lying areas have little regional gradient and thick till cover, which causes poor drainage and results in wetland environments with perched water tables and dense vegetation (Rice et al., 2017). The highlands typically have low shrubs, although some

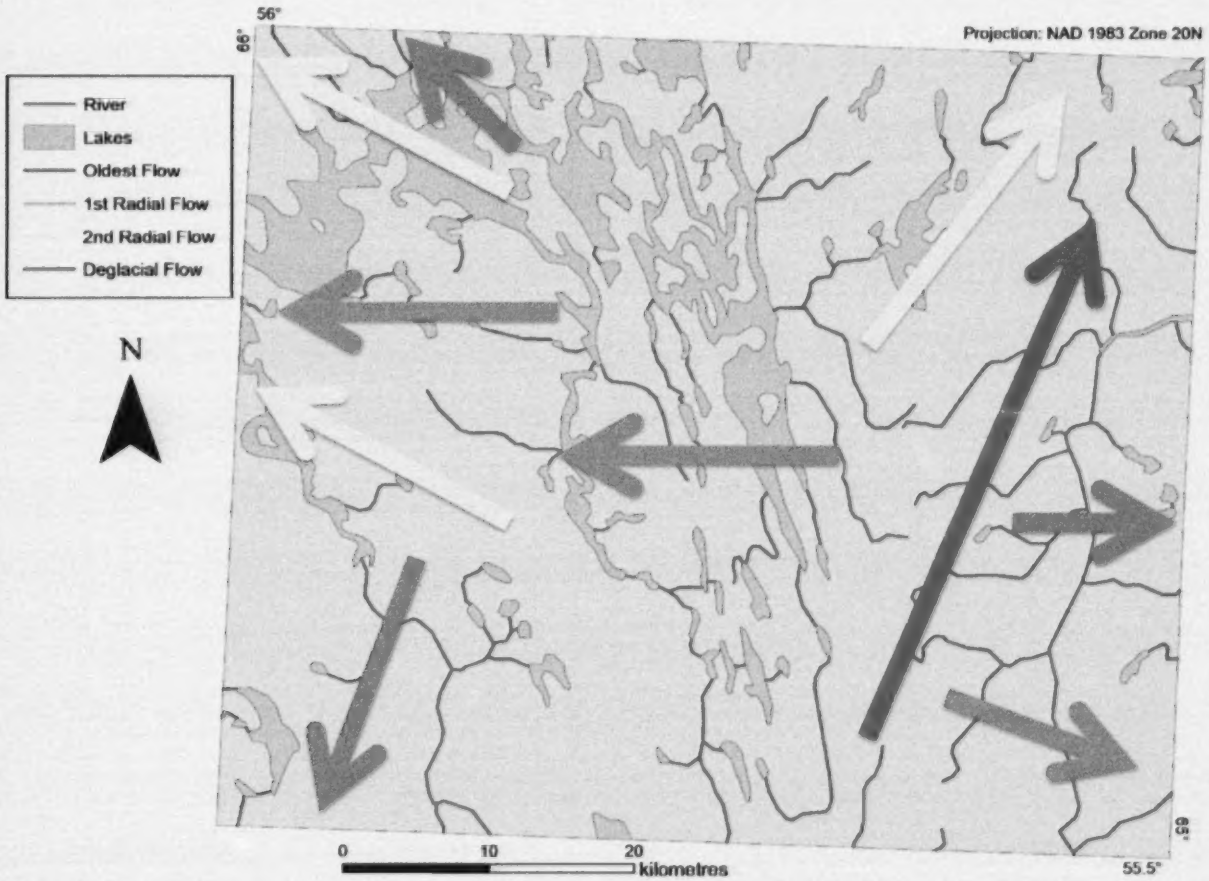

Figure 5. Map showing ice flow in the study area. The oldest phase was to the northeast (red), followed by two radial phases, the first to the west and southeast (orange) and the second to the northwest and northeast (yellow). The final deglacial stage was to the south–southeast and northwest (purple) (Rice et al., 2016).

areas have stunted coniferous trees, which could influence gamma-ray readings.

Deglacial sediments also dominate portions of the study area. At higher elevations, glaciofluvial meltwater corridors influence the surficial geology through erosion. The result is variably decreased depths of sediment cover within the corridors. At lower elevations, boulder lags and winnowed till surfaces occur as the result of glacial Lake McLean. This deglacial lake inundated the northwest part of the study area during ice retreat (Ives, 1960; Barnett, 1967; Jansson, 2003; Rice et al., 2017).

METHODS

Available airborne GRS data covers the entire study area at 200 m line-spacing. Field measurements by ground GRS were obtained on till and bedrock surfaces; till samples were collected and analyzed in the gamma-ray laboratory at the Geological Survey of Canada (GSC) in Ottawa. Potassium concentration values are reported as percentage of total mass. Uranium and thorium concentrations are measured from daughter products of their respective decay chains and are therefore reported in equivalent units (eU and eTh) (International Atomic Energy Agency, 2003). An 'equivalent' unit of measurement is required as the actual amount of primary radioelement is presented under the assumption of radioactive equilibrium with daughter products (International Atomic Energy Agency, 2003). The data collection methodology is further described below.

Airborne gamma-ray spectrometry

Airborne GRS was collected as part of the Quebec Ministry of Natural Resource's Romanet Lake airborne geophysical survey (D'Amours and Intissar, 2013). These airborne measurements of potassium, equivalent uranium, and equivalent thorium were used by the GSC to create a ternary diagram (Fig. 6) (McClenaghan et al., 2016) in which potassium (K), equivalent uranium (eU) and equivalent thorium (eTh) concentrations are represented by the colours magenta, cyan and yellow,

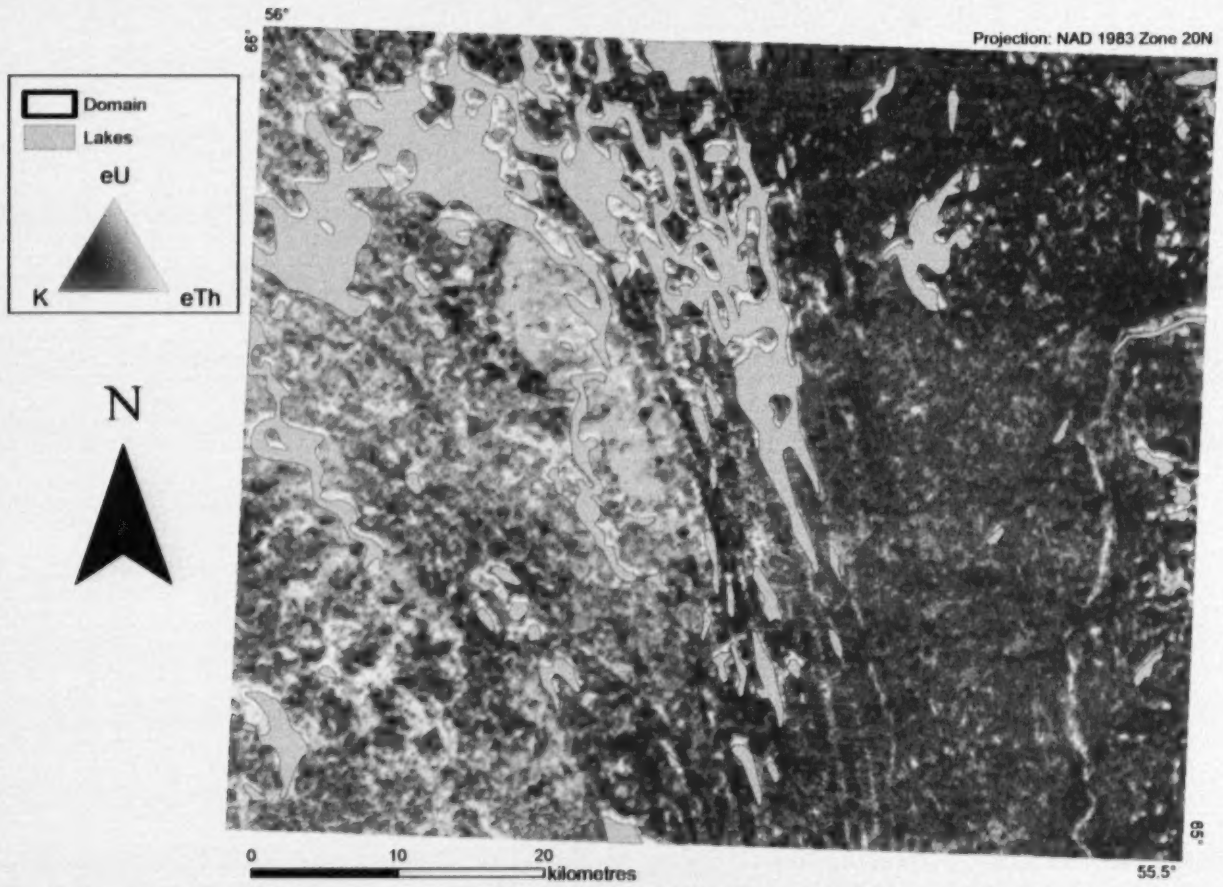

Figure 6. Map of the study area shaded using the ternary diagram of the airborne gamma-ray spectrometry response (Fortin, et al., 2015). The colour shown at any location reflects the relative surface concentration of potassium (K), equivalent uranium (eU), and equivalent thorium (eTh) represented in the ternary diagram by magenta, cyan, and yellow, respectively (Broome et al., 1987).

respectively. At any location on the diagram, the colour combination reflects the relative proportion of potassium, equivalent uranium, and equivalent thorium concentrations in the surface materials (Broome et al., 1987).

For example, if potassium makes up the whole response (i.e. no equivalent uranium or equivalent thorium), the colour would be pure magenta; however, an area with similar contributions from potassium and equivalent uranium and no equivalent thorium would display as blue (a combination of magenta and cyan, and no yellow). Additionally, the total signal magnitude of an area scales the resulting colour saturation (Broome et al., 1987). Strong responses have a more vibrant colour, making them appear crisp, whereas locations with a weak airborne response have a white or duller colour. As a result, whiter areas indicate a lack of GRS signal, whereas crisp colours signify a strong gamma-ray output received from the surface.

The ternary diagram was used to manually delineate qualitative radiometric domains over the study area. Domains were differentiated primarily on ternary colour and strength of response (Campbell et al., 2007; Fortin et al., 2015), although bedrock geology, surficial geology, and topography were also referenced. Manual tracing of domains can be subjective but is based on distinctive contrasts in the shading from a ternary diagram. Radiometric domains can be traced in different ways depending on the discriminating factor that is used or the spatial scale required but domains should always express a definite link between the source material and the domain signature. The data presented here is an interpretation at a relatively small scale, covering the northwest corner of NTS Sheet 23P, but the domain procedure will be completed for the larger study area at a future date (McClenaghan et al., 2016).

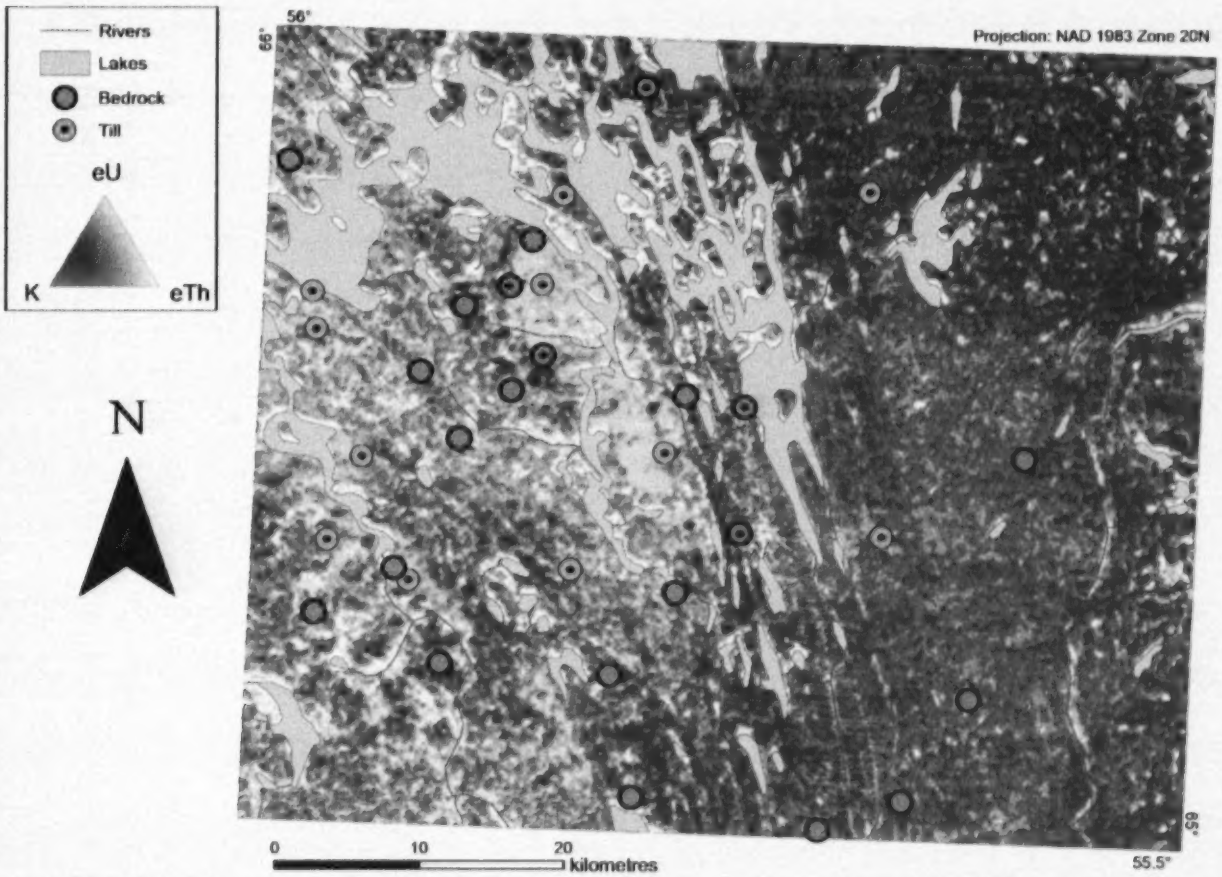

Figure 7. Map shaded using the ternary diagram of the airborne gamma-ray spectrometry response (Fortin, et al., 2015) showing the location of all ground gamma-ray spectrometry (GRS) measurements that were taken using a handheld GRS.

Ground gamma-ray spectrometry

Field sites were selected based on the regional surficial mapping conducted by the GSC, which was influenced by the mineral potential of the bedrock, accessibility via helicopter, and potential for ice-flow indications (Fig. 7) (Rice et al., 2016). A RS-230 BGO Super-Spec (Radiations Solutions Inc.) portable gamma-ray spectrometer was used to collect ground measurements at field sites within the study area (Fig. 8).

The RS-230 detector is a 103 cm^3 bismuth germanate oxide crystal and the 'assay' mode was used for all measurements (Radiation Solutions Incorporated, 2016). This mode records concentrations of potassium, equivalent uranium, and equivalent thorium, relying on user-defined calibration parameters. The two materials that were measured were bedrock outcrop and surface till. At locations where both were present at surface, a recording of each was taken for comparison. At each site, efforts were undertaken to reduce undesirable influences by maximizing distance from water and clearing the ground of vegetation. After successful spectral stabilization of the instrument to the surrounding background gamma-rays, the handheld GRS unit was placed on the ground surface with the sensor facing down for five minutes. The cumulative potassium, equivalent uranium, and equivalent thorium concentrations of the top 0.3 to 0.5 m of till or bedrock were recorded (Fig. 8). These values were then documented and a photo was taken of the RS-230 BGO Super-Spec in its assay location. General field observations were also recorded, noting the weather at the time of the reading, topography, and surficial geology. Appendix A1 contains a table of the ground till and bedrock handheld GRS results.

Laboratory gamma-ray spectrometry

Till samples were collected at most GRS field sites for lab analysis (Fig. 9). Following guidelines outlined in Spirito et al. (2011) and McClenaghan et al. (2013), with specific methodology for this region outlined by Rice et al. (2016), unweathered C-horizon material was sampled and equipment was cleaned between sites to reduce cross-contamination. The typical depth for sam-

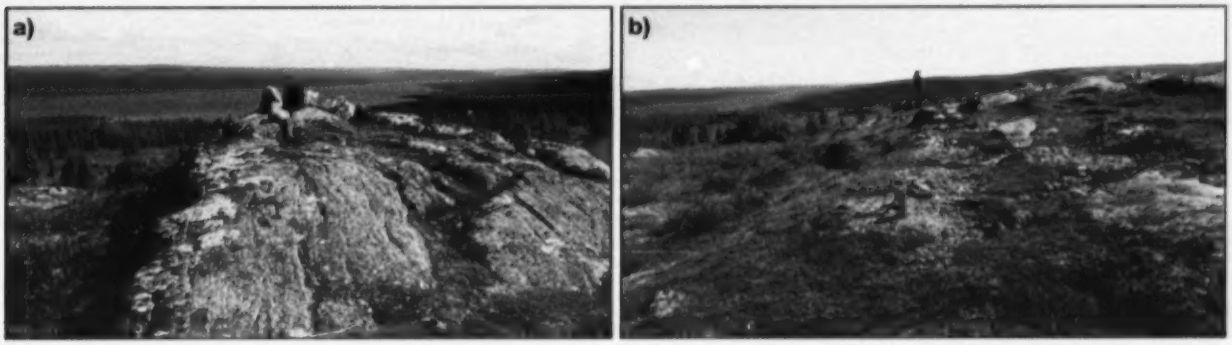

Figure 8. a) Photograph of the RS-230 BGO Super-Spec taking gamma-ray readings on the bedrock outcrop at site 16-PTA-063. This is a typical example of bedrock at surface in the study area. **b)** Photograph of the same instrument recording gamma-ray readings on a till veneer (typically less than 2 m thick), also at site 16-PTA-063. When possible, readings were taken on fresh mudboils, as is shown in this photograph. However, if mudboils were not present, readings for till were taken on a cleared area of the ground in order to get the most accurate readings while minimizing the disturbance of vegetation.

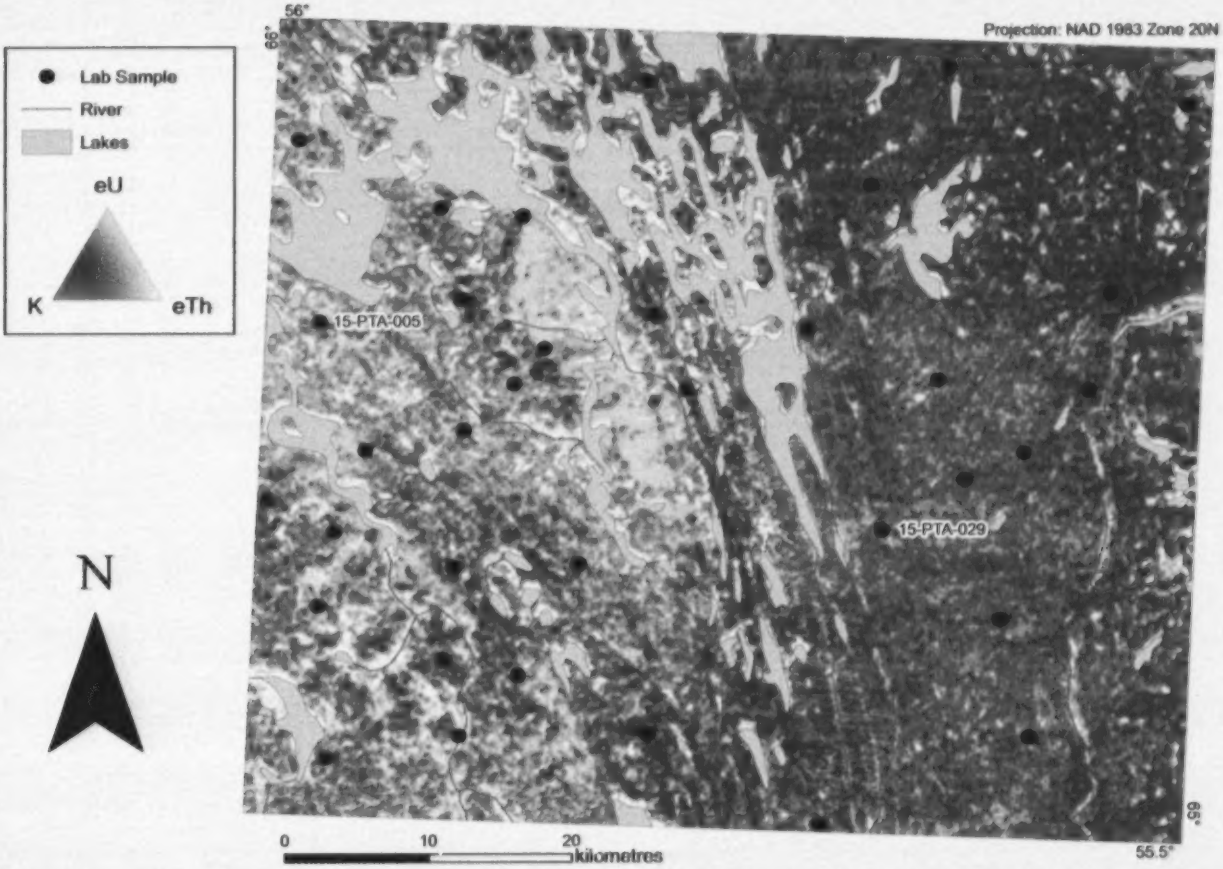

Figure 9. Map shaded using the ternary diagram of the airborne gamma-ray spectrometry response (Fortin, et al., 2015) showing the locations of sites where till samples were collected. These samples were later analyzed in the GSC Spectrometry Laboratory in Ottawa.

pling was above the 0.5 m penetration depth of the GRS instrument, as this area had mudboils bringing C-horizon material to surface. These till samples were shipped to the Geological Survey of Canada Sedimentology Laboratory in Ottawa. The samples were prepared for gamma-ray laboratory analysis by drying the material and then filling 10 cm-diameter sample tins. This was done for both the bulk and <2 mm size fraction of the sample. The tins were then left for three weeks to allow radioactive equilibrium to be reached. Once prepared, the samples were processed at the Geological Survey of Canada Gamma-ray Spectrometry Laboratory in Ottawa (Fig. 10). Assay time for each tin was 20 minutes, recording the 3 major radioelement concentrations. The stability of the laboratory GRS measurements was validated using a Cesium-137 standard at the start of every measurement session as well as standards of distilled water, potassium, uranium, and thorium at the start and end of every session. The laboratory measurements can be traced to reference materials RGK-1, RGU-1 and RGTh-1 (International Atomic Energy Agency, 1987). Only the bulk sample results were used for analysis as these give a more accurate representation of the native till that the field GRS (airborne and ground) would be recording. These lab GRS results can be found in Appendix A2.

Figure 10. a) Photograph showing a tin that has been filled with dried till. These samples were analyzed for potassium, equivalent uranium, and equivalent thorium contents. **b)** Photograph showing the gamma-ray spectrometer at the Geological Survey of Canada GRS laboratory, Ottawa that was used for analyses. Samples are loaded on the sample changer and fall into the chamber below to be analyzed (instrument in bottom right of the image). The values are then logged in the computer on the left.

Pebble lithologies

As Overburden Drilling Management processed the indicator mineral samples; clasts larger than 5.6 mm were separated. An acid solution was used to wash the clasts to remove cemented matrix and any oxidation staining on their surface. The cleaned clasts were then coned and quartered, resulting in the sorting of about 350 clasts per site. A subset of the samples collected at 35 sites within the study area was selected from those compiled as part of the larger GEM2 Hudson-Ungava project (Rice et al., 2017). The classification scheme consisted of 16 different lithologies; each clast was sorted into a single category. The lithologies used were 1) mafic intrusive, 2) intermediate intrusive, 3) felsic intrusive, 4) leucogranite, 5) ultramafic, 6) Doublet Zone metavolcanic , 7) metasedimentary, 8) Laporte Domain rocks (granite with muscovite), 9) Lac Zeni amphibolite, 10) vein quartz, 11) quartzite, 12) Mistinibi paragneiss (migmatite), 13) Michikmau intrusive (granite and anorthosite), 14) Juillet syenite, 15) iron formation (oolitic Jasper, banded to massive magnetite/hematite, and specularite), and 16) others (Rice et al., 2017). These 16 classifications reflect the regional bedrock lithologies (Sanborn-Barrie, 2016).

Data compilation

Elevation, bedrock geology, ice-flow history, and radioelement concentrations were compiled in ArcGIS. Radiometric domains were delineated based on the map shading according to the K-eU-eTh ternary diagram (Fig. 6), and the averages obtained from the potassium, equivalent uranium, and equivalent thorium readings within each domain (Campbell et al., 2007; Fortin et al., 2015). Additionally, values for airborne, in situ bedrock, in situ till, and lab samples were plotted and compared. The airborne value used was the airborne GRS concentration associated with the sampling point for the other GRS method. The graphs created were utilized for correlation analysis and insight into the relationships among the GRS data sources.

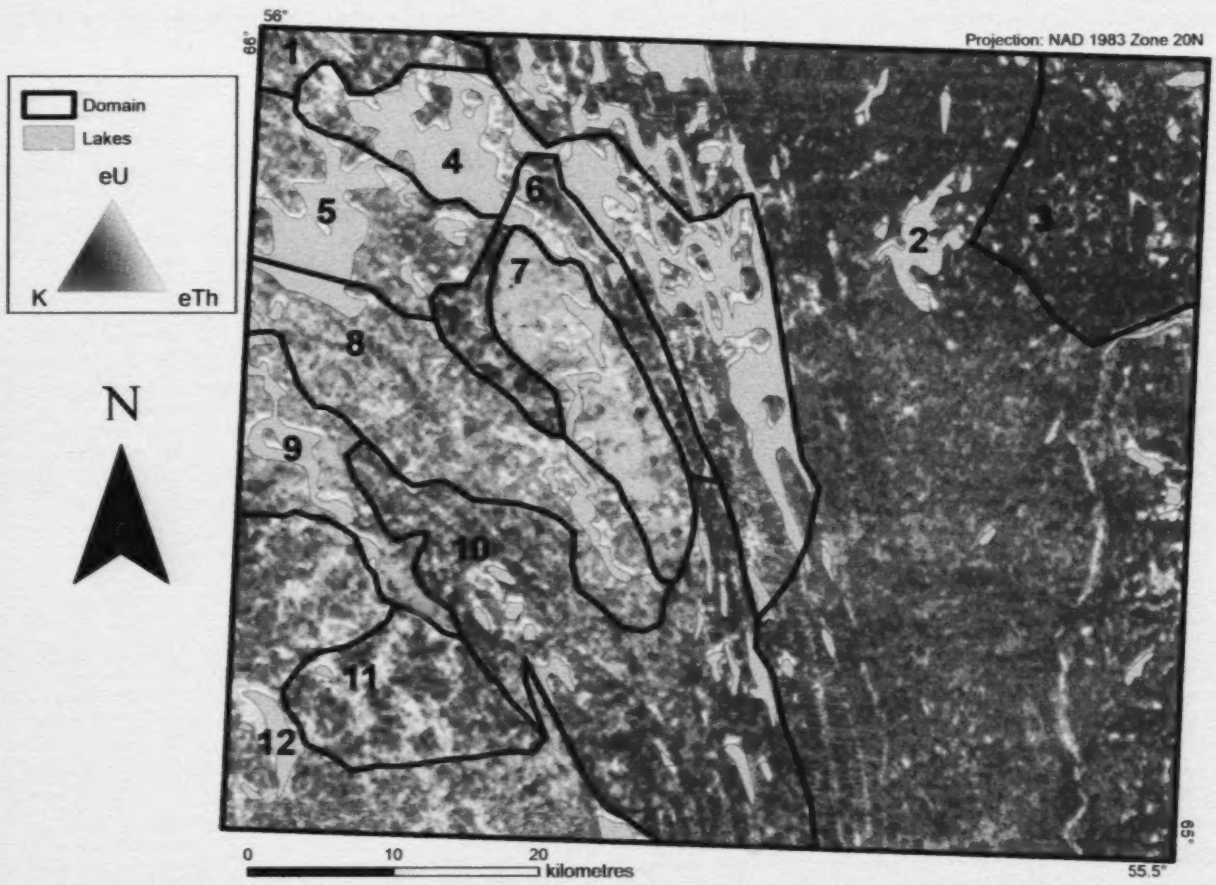

Figure 11. Map shaded using the ternary diagram of the airborne gamma-ray spectrometry response (Fortin, et al., 2015) showing the interpreted radiometric domains, which have been divided based on airborne gamma-ray spectrometry measurements. The number contained within each domain indicates its name.

RESULTS

Domain separation

Twelve radiometric domains were manually and qualitatively delineated by identifying areas of similar airborne radiometric response (Fig. 11). Domains 1, 6, and 10 are all a similar purple and blue, indicating potassium and equivalent uranium are the main radioelements present (Fig. 11). Domain 2 is mostly magenta, indicating a large potassium content, although some minor amounts of uranium are present. Domain 3 is distinguished by having more red, which corresponds to mainly potassium and equivalent thorium. Domains 4 and 8 are characterized by relative light responses, meaning a weak gamma-ray signal. Domain 8 is more dotted with areas of weak response compared to Domain 4, where large areas are signal void. Domains 4 and 8 tend to have potassium as the major contributor to the gamma-ray signature but are quite variable overall, especially within Domain 8 (Fig. 11). Domains 5, 7, and 9 are green, indicating a composition characterized mainly by their equivalent thorium and equivalent uranium relative concentrations. Domain 11's blue colour indicates equivalent uranium and potassium with equivalent uranium more characteristic of the signature (Fig. 11). Domain 12 has a cyan colour, meaning uranium is the main source of gamma rays in this domain, with some green indicating relatively small amounts of thorium (Fig. 11). Table 1 summarizes the average potassium, equivalent uranium, and equivalent thorium readings from the airborne, ground, and laboratory gamma-ray measurements for all radiometric domains. The local bedrock geology that underlies each domain is presented in Figure 12. Detailed descriptions of the airborne radiometric properties, underlying bedrock, elevation, and surficial geology for each of the radiometric domains are provided below and summarized in Table 2.

Domain 1

Located in the northwest corner of the study area, Domain 1 is the smallest, with a total area of 50 km^2.

Table 1. Average values for readings from airborne, bedrock, ground till ($Till_G$) and laboratory till ($Till_L$) by domain. "-" indicates that no values were recorded in that domain. Averages for airborne values were obtained by averaging the individual cell values for all cells within a domain. Averages for all other data sources were completed by dividing the values given by the number of measurements (n).

Domain	Airborne			Bedrock			$Till_G$			$Till_L$		
	K (%)	eU (ppm)	eTh (ppm)	K (%)	eU (ppm)	eTh (ppm)	K (%)	eU (ppm)	eTh (ppm)	K (%)	eU (ppm)	eTh (ppm)
1	0.7	0.5	1.9	- (n=0)	- (n=0)	- (n=0)	- (n=0)	- (n=0)	- (n=0)	- (n=0)	- (n=0)	- (n=0)
2	1.0	0.3	2.3	2.0 (n=4)	0.6 (n=4)	19.4 (n=4)	1.6 (n=3)	0.5 (n=3)	3.2 (n=3)	2.0 (n=11)	1.2 (n=11)	6.0 (n=11)
3	1.3	0.5	3.7	- (n=0)	- (n=0)	- (n=0)	- (n=0)	- (n=0)	- (n=0)	2.1 (n=2)	1.0 (n=2)	5.4 (n=2)
4	1.9	0.2	1.2	2.8 (n=1)	28.8 (n=1)	0.4 (n=1)	1.9 (n=1)	0.6 (n=1)	4.3 (n=1)	- (n=0)	- (n=0)	- (n=0)
5	0.6	0.4	2.7	1.3 (n=1)	1.9 (n=1)	6.8 (n=1)	- (n=0)	- (n=0)	- (n=0)	2.4 (n=2)	2.5 (n=2)	12.7 (n=2)
6	0.8	0.5	2.8	3.7 (n=2)	3.2 (n=2)	7.1 (n=2)	1.2 (n=1)	0.7 (n=1)	3.1 (n=1)	1.9 (n=4)	1.4 (n=4)	6.5 (n=4)
7	0.9	1.0	6.0	2.4 (n=3)	4.3 (n=3)	21 (n=3)	1.8 (n=4)	1.7 (n=4)	10.5 (n=4)	1.8 (n=1)	1.4 (n=1)	5.8 (n=1)
8	0.6	0.3	2.0	1.1 (n=4)	0.5 (n=4)	1.1 (n=4)	1.3 (n=2)	0.4 (n=2)	3.7 (n=2)	1.8 (n=3)	1.3 (n=3)	7.3 (n=3)
9	0.8	0.6	3.8	4.0 (n=1)	8.3 (n=1)	40 (n=1)	1.6 (n=2)	1.0 (n=2)	4.1 (n=2)	2.0 (n=2)	1.7 (n=2)	6.3 (n=2)
10	0.9	0.4	2.5	2.3 (n=4)	1.9 (n=4)	5.4 (n=4)	1.8 (n=2)	1.6 (n=2)	5.4 (n=2)	2.1 (n=4)	1.2 (n=4)	5.9 (n=4)
11	0.8	0.6	2.7	2.3 (n=1)	3.2 (n=1)	7.2 (n=1)	1.3 (n=1)	1.2 (n=1)	3.9 (n=1)	2.1 (n=3)	1.6 (n=3)	6.5 (n=3)
12	0.8	0.8	3.2	2.6 (n=1)	3.1 (n=1)	8.1 (n=1)	1.8 (n=1)	2.7 (n=1)	6.6 (n=1)	2.3 (n=3)	2.7 (n=3)	7.6 (n=3)

It has a distinctive blue colour, indicating a potassium and equivalent uranium content at the surface (Fig. 11). Although similar in total airborne response to Domain 2, it contains slightly higher levels of equivalent uranium (0.5 ppm) and less potassium (0.7%) (Table 1). The underlying bedrock is quartzofeldspathic gneiss, with the border separating it from Domain 2 aligning with the bedrock contact to the greywacke, shale, and biotite schist unit (Fig. 12). Additionally, Domain 1 is topographically lower than Domain 2 (Fig. 4). This area was heavily influenced by the northwest ice flow in the region (Fig. 5) and surface sediments are dominantly till veneer (Rice et al., 2017). There are no ground-based or laboratory measurements taken within this domain, so comparisons with GRS methods was not completed (Fig. 7, 9).

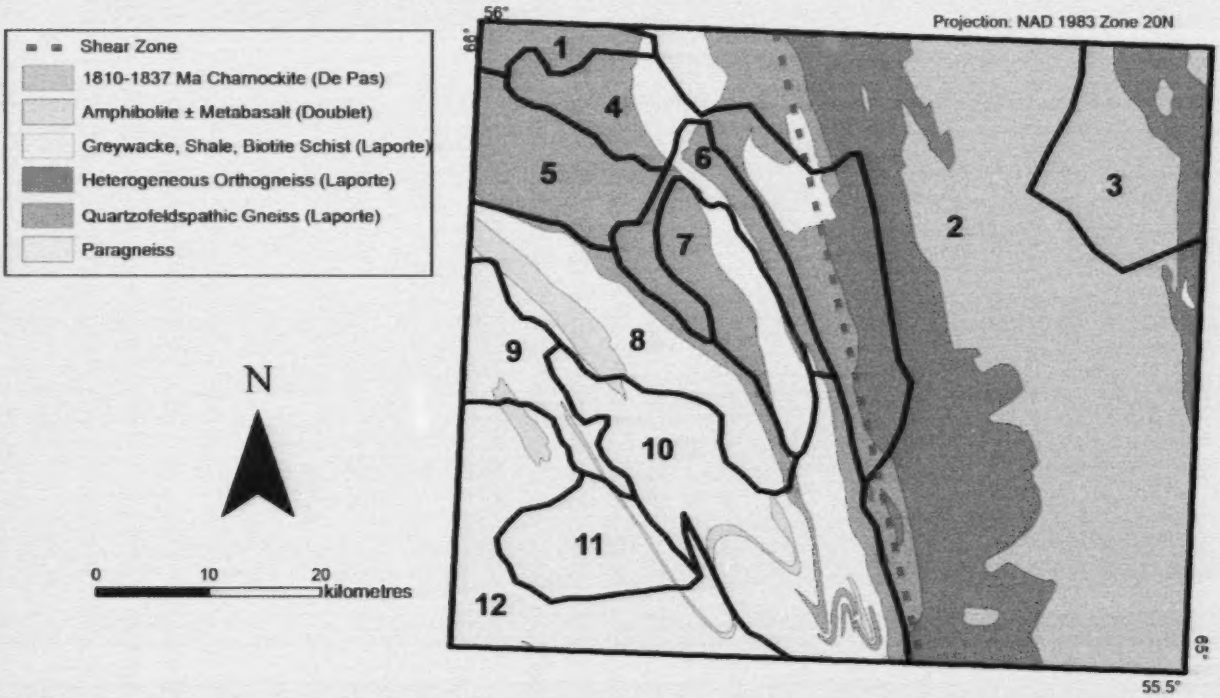

Figure 12. Map of the study area showing the domain boundaries superimposed on a map of the bedrock geology (Sanborn-Barrie, 2016).

Table 2. General characteristics of the 12 radiometric domains classified in the study area. The topography of a domain was categorized as low, intermediate, or high based on observations from the DEM. Low-lying areas had typical elevations that ranged from 307 to 426 m ALS, intermediate domains had elevations between 426 and 546 m ASL, and high elevations were classified as 546 to 666 m ALS. Surficial geology presented is from Rice et al. (2017).

Domain	Ternary map hue	Radioelement average values	Predominant bedrock unit	Elevation	Surficial geology	Comments and correlations
1	Blue	Potassium + uranium **K (%) – 0.7** **eU (ppm) – 0.5** eTh (ppm) – 1.9	Quartzofeldspathic gneiss	Intermediate	Till veneer	- Small portion in northwestern corner of study area - Discriminated based on higher uranium content than surroundings - Only airborne readings available
2	Purple/ Blue	Potassium + uranium **K (%) – 1** **eU (ppm) – 0.3** eTh (ppm) – 2.3	Heterogeneous orthogneiss + charnockite	High	Till veneer, bedrock outcrop, meltwater channels, and glaciofluvial deposits	- Largest domain covering the eastern side of the study area - Based on higher potassium content - Correlated to the bedrock sources being exposed at high elevations
3	Red	Potassium + thorium **K (%) – 1.3** eU (ppm) – 0.5 **eTh (ppm) – 3.7**	Heterogeneous orthogneiss	High	Till veneer and bedrock outcrop	- Small domain located in the northeastern portion of the study area - Separated due to higher thorium content compared to surrounding Domain 2 - Associated loosely with bedrock contact on eastern side of De Pas Batholith with orthogneiss contact
4	White/ Purple	Low response/ potassium **K (%) – 1.9** eU (ppm) – 0.2 eTh (ppm) – 1.2	Greywacke, shale, biotite schist	Low	Till veneer, till blanket, and organic material	- Weak airborne GRS response is likely correlated to the low topography and large amounts of surface water absorbing gamma rays - Thicker vegetation cover - Winnowed sediments
5	Green	Uranium + thorium K (%) – 0.6 **eU (ppm) – 0.4** **eTh (ppm) – 2.7**	Quartzofeldspathic gneiss	Low	Till veneer, bedrock outcrop, and organic material	- Located in northwestern portion of the study area - May have same bedrock source as Domains 7 and 9 because of similar responses - Northwest-southeast drumlinoid features present
6	Blue	Potassium + uranium **K (%) – 0.8** **eU (ppm) – 0.5** eTh (ppm) – 2.8	Quartzofeldspathic gneiss	High	Till veneer and bedrock outcrop	- Correlated to a topographic high that encompasses Domain 7 - Discriminated based on higher uranium response with some potassium - Boulder lag beach ridges present - Winnowed sediments
7	Green	Uranium + thorium K (%) – 0.9 **eU (ppm) – 1** **eTh (ppm) - 6**	Quartzofeldspathic gneiss + greywacke, shale, biotite schist	Intermediate	Till veneer and till blanket	- Large strong homogeneous uranium and thorium response - Possible correlation to Domains 5 and 9
8	White/ Green/ Purple	Low response/ potassium **K (%) – 0.6** eU (ppm) – 0.3 eTh (ppm) - 2	Greywacke, shale, biotite schist + amphibolite with metabasalt	High	Till veneer and till blanket	- Weak airborne response - Northern border follows contact of greywacke, shale, biotite schist and quartzofeldspathic gneiss
9	Green	Uranium + thorium K (%) – 0.8 **eU (ppm) – 0.6** **eTh (ppm) - 3.8**	Greywacke, shale, biotite schist	Low	Till blanket	- Similar in composition to Domains 5 and 7 - Follows orientation of lake - Separated from surroundings based on strong uranium and thorium response
10	Purple/ Blue	Potassium + uranium **K (%) – 0.9** **eU (ppm) – 0.4** eTh (ppm) – 2.5	Greywacke, shale, biotite schist	High	Till veneer and till blanket	- Similar in composition to Domain 2, separated based on higher uranium contents - Follows a topographic high - Sediment cover gets thicker in western arm
11	Blue	Potassium + uranium **K (%) – 0.8** **eU (ppm) – 0.6** eTh (ppm) – 2.7	Greywacke, shale, biotite schist	Intermediate	Till blanket	- Similar to Domain 12, differentiated based on higher potassium content
12	Cyan	Uranium K (%) – 0.8 **eU (ppm) – 0.8** eTh (ppm) – 3.2	Greywacke, shale, biotite schist	Intermediate	Till blankets and bedrock outcrop	- Located in southwestern portion of the study area - Delineated based on high uranium only content

Domain 2

Domain 2 spans the entire study area from north to south and is the largest domain, with an area of 1502 km^2. This domain is predominantly magenta with some patches of blue (Fig. 11). The colouring reflects the high potassium content (1.0%) with, locally, some equivalent uranium (0.3 ppm) relative to equivalent thorium (Table 1). The domain's western border follows the north-south boundary that divides the bedrock geology and topography (Fig. 4, 12). This domain is underlain by the De Pas Batholith (Fig. 12), has a high elevation (Fig. 4), and the surficial geology is dominantly till veneers with bedrock outcrops on topographic highs. This area also contains many glaciofluvial features, including meltwater channels and sporadic outwash deposits (Rice et al., 2017).

Domain 3

Located in the northeastern corner of the study area, Domain 3 was delineated based on its red colour, which corresponds to higher thorium content (3.7 ppm) than other units (Fig. 11, Table 1). Domain 3 is underlain by heterogeneous orthogneiss bedrock (Fig. 12) and is at a similar elevation as Domain 2 (Fig. 4). Surficial cover in this domain is dominated by till veneer, although sporadic outcrops are present (Rice et al., 2017).

Domain 4

Domain 4 has a white and light purple response (Fig. 11), which is a result of a high potassium average (1.9%) and significant signal attenuation (Table 1). This domain does not correlate well with the underlying bedrock units (greywacke, shale, and biotite schist) (Fig. 12) and is at a relatively low elevation with undulating terrain containing numerous lakes that reduce the gamma-ray response (Fig. 4). The surficial geology of this domain is characterized by till veneer on the highlands and till blankets in the valleys with significant organic deposits (Rice et al., 2017). These wet organics also contribute to the attenuation of the gamma-ray signal, particularly in the northern portion of the domain. Surface sediments within were winnowed by glacial Lake McLean. The weak and somewhat variable gamma-ray signature of this area makes it difficult to discriminate from or correlate with neighbouring areas, and as such, it was grouped together as an undefined area.

Domain 5

Located in the northwestern portion of the study area, Domain 5 displays a green colour, indicating higher concentrations of equivalent uranium (0.4 ppm) and equivalent thorium (2.7 ppm) relative to potassium (Fig. 11, Table 1). It has similar readings as Domain 7, although disconnected by Domain 6. Domain 5 has quartzofeldspathic gneiss bedrock outcrops (Fig. 12), with low-lying areas that are covered by till veneers and organic deposits. This domain also contains many drumlinoid features oriented toward the northwest, which are associated with the third ice-flow phase (Fig. 5) (Rice et al., 2016).

Domain 6

Wrapping around Domain 7, Domain 6 was differentiated from its surroundings based on its blue colour (Fig. 11), which is supported by its airborne averages of relatively higher potassium and equivalent uranium readings to equivalent thorium (Table 1). Domain 6 is underlain by quartzofeldspathic gneiss (Fig. 12) and follows a topographic high (Fig. 4). Additionally, this domain contains a large number of bedrock outcrops and was affected by glacial Lake Mclean, producing boulder lags as beach ridges and thin layers of winnowed till at lower elevations (Rice et al., 2017).

Domain 7

Located near the centre of the study area, Domain 7 has a vibrant green colour indicating a strong signal response for equivalent thorium (6 ppm) and equivalent uranium (1 ppm) (Fig. 11, Table 1). The domain does not match any specific bedrock units (Fig. 12), is at intermediate topographic elevation (Fig. 4), and is covered predominantly by till veneer with some areas covered by a till blanket (Rice et al., 2017).

Domain 8

Domain 8 has a pale tone indicating a weak overall response (Fig. 11). The domain is green in the north and purple in the south, indicating the majority of this weak response is coming from changing potassium levels that decrease to the north where the signal is dominated by equivalent uranium (Fig. 11, Table 1). The northern border follows the bedrock contact between the Laporte Domain metasedimentary unit and quartzofeldspathic gneiss to the east; the domain is underlain primarily by greywacke, shale, and biotite schist (Fig. 12). Domain 8 has an intermediate topography with a thin quartzite ridge (Fig. 4) and is characterized by till veneers on uplands and till blankets in lowlands. There are also significant meltwater channels and glaciofluvial deposits within this domain (Rice et al., 2017).

Domain 9

Domain 9 is characterized by a green colour, indicating high equivalent uranium (0.6 ppm) and equivalent thorium (3.8 ppm) content (Fig. 11). The bedrock underlying this area is greywacke, shale, and biotite schist (Fig. 12). The terrain is at low elevation with little

topographic variation (Fig. 4), and is predominantly covered by till blankets (Rice et al., 2017). This domain follows the southeast orientation of the lake contained within it.

Domain 10

Domain 10 has a purple-blue colour, indicating that potassium (0.9%) and equivalent uranium (0.4 ppm) concentrations are higher relative to thorium (Fig. 11). The underlying bedrock is mostly Laporte Domain metasedimentary rocks, with the eastern border aligning with its contact with the quartzofeldspathic unit (Fig. 12). This domain has overall high topographic elevation with a dominant topographic ridge and numerous bedrock outcrops (Fig. 4). Adjacent low-lying areas are generally covered by a till veneer that thickens in the western portion of the domain (Rice et al., 2017).

Domain 11

Domain 11 has a dominant blue colour, indicating high potassium (0.8%) and equivalent uranium (0.6 ppm) content (Fig. 11, Table 1). This domain is characterized by greywacke, shale, and biotite schist bedrock (Fig. 12), an intermediate topographic elevation (Fig. 4), and is covered by till blanket deposits (Rice et al., 2017).

Domain 12

Domain 12, located in the southwestern corner of the study area, is defined by a cyan colour, indicating high equivalent uranium (0.8 ppm) content relative to potassium and thorium (Fig. 11, Table 1). The bedrock unit, elevation, and surficial geology are very similar to those in Domain 11 — underlain by Laporte Domain metasedimentary rocks (Fig. 12), at intermediate elevation (Fig. 4), and till blankets cover the majority of the area — however, Domain 12 has more bedrock exposed at surface (Rice et al., 2017).

In summary, the domains in the western portion of the study area have a similar northwest–southeast orientation (Fig. 11), which is consistent with the structure of the bedrock geology, landforms, and prominent ice-flow directions (Fig. 5, 12). The size of the domains varies, with Domain 1 being the smallest and Domain 2 being the largest. Except for Domain 2 where the De Pas River has down cut through the landscape, the topography within a domain is consistent (Fig. 4). Typically, bedrock units do not align with the domain boundaries, although some domain borders coincide with bedrock contacts (i.e. Domains 1, 2, and 3; Fig. 12). The surficial materials vary from one domain to another but are consistent within a domain.

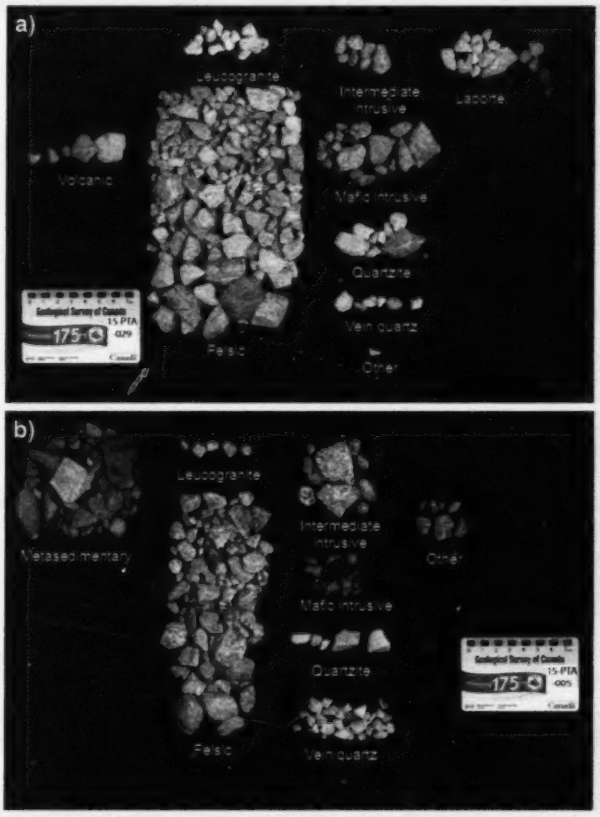

Figure 13. Photographs of pebble counts of till samples **(a)** 15-PTA-029 and **(b)** 15-PTA-005. A comparison of these photographs shows a decrease in the quantity of felsic intrusive pebbles and an increase in metasedimentary pebbles with increasing distance from the De Pas Batholith. Photographs by J. Rice.

Pebble counts

The quantities of felsic intrusive pebbles in the till decreased with increasing distance from the De Pas Batholith. For example, sample 15-PTA-029, collected directly on the batholith, has a till consisting of 77% felsic pebbles compared to 47% in sample 15-PTA-005, collected 40 km from the batholith, on the Laporte Domain (Fig. 4, 13). These samples also show a large variation in the number of metasedimentary clasts observed: sample 15-PTA-005 having 98 and sample 15-PTA-029 having none. This difference indicates a change in the source of the till from the De Pas Batholith to the Laporte Domain. The results show a trend toward locally sourced tills, which is reflected in the majority of the clasts matching proximal bedrock lithologies (Rice et al., 2017). Sample 15-PTA-005, collected over the Laporte Domain, contains metasedimentary clasts, and sample 15-PTA-029, collected over the De Pas Batholith, contains felsic intrusive clasts. This trend is observed throughout the dataset.

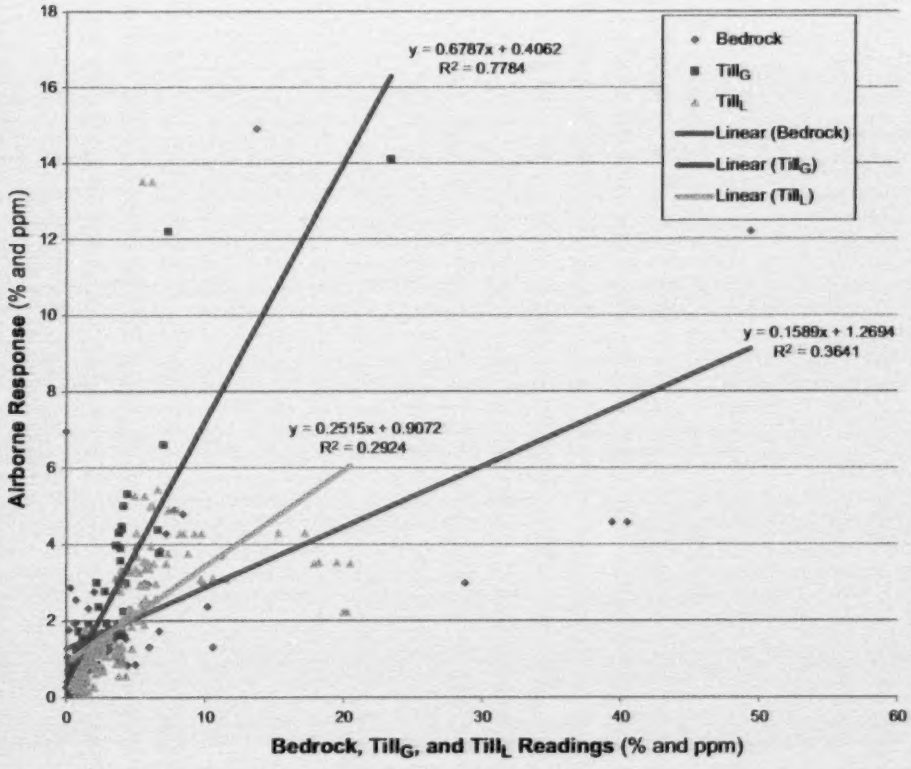

Figure 14. Scatterplot of bedrock (n = 66), till response measured on the ground ($Till_G$; n = 51), and till response measured in the laboratory ($Till_L$; n = 105) against the corresponding airborne radiometric concentration values. X-axis represents values from each different measurement type against its corresponding airborne value. The line-of-best-fit has also been included with its equation as well as the R^2 values. The ground measurements of till best align with their airborne response.

Comparison of gamma-ray spectrometry datasets

Comparison of in situ bedrock, in situ till, and laboratory till GRS to airborne radiometric values was completed to test for correlations (Fig. 14). Any linkages that could be identified would help in determining the origin of the different signals. For example, if the bedrock response is similar to the airborne response, then it would have a high influence on the airborne readings and would result in a close linear relationship. The analysis was limited to simple linear regression to identify only the main relationships. When the handheld ground surface till values are plotted against the airborne response, the best linear regression was observed ($R^2 = 0.78$) (Fig. 14). For bedrock values, an R^2 value of 0.36 was found when plotted against the airborne readings (Fig. 14). Laboratory bulk till samples had an R^2 value of 0.29 (Fig. 14). These trends are also observed individually for potassium, equivalent uranium, and thorium throughout the datasets, although the R^2 values differ.

All other combinations of GRS results showed no major relationships in R^2 values. Bedrock versus ground till had an R^2 of 0.38 (Fig. 15), bedrock to laboratory samples recorded R^2 values of 0.04 (Fig. 16), and ground till to laboratory till results showed an R^2 of 0.37 (Fig. 17).

DISCUSSION

Radiometric domain gamma-ray response

Correlation of gamma-ray airborne response with bedrock geology has been observed, especially when only a thin layer of unconsolidated material overlies the bedrock surface (Guastaldi et al., 2013; Youssef and Elkhodary, 2013; Beamish, 2016; Youssef, 2016). A similar correlation is observed within the study area, specifically for Domains 2 and 3. Both domains are characterized by high elevations and more rugged relief, which coincides with abundant bedrock outcrops at the surface (Table 2) (Rice et al., 2016, 2017). Furthermore, within Domain 2, potassium concentrations obtained from ground GRS in till (1.6%) is comparable to measurements obtained on bedrock surfaces (2%), where comparatively low values of equivalent uranium concentrations are measured (Table 1). These measurements are consistent with the magenta to red hue that can be seen on the image (Fig. 9). The high potassium can be partly explained by the high K-feldspar component (Sanborn-Barrie, 2016) within the De Pas Batholith, which underlies these domains and outcrops frequently or is found above the 0.5 m penetration depth of GRS instruments.

The homogeneous GRS responses of Domains 2 and 3 implies that till in the upland region of the De Pas Batholith is locally derived and has similar radioelement

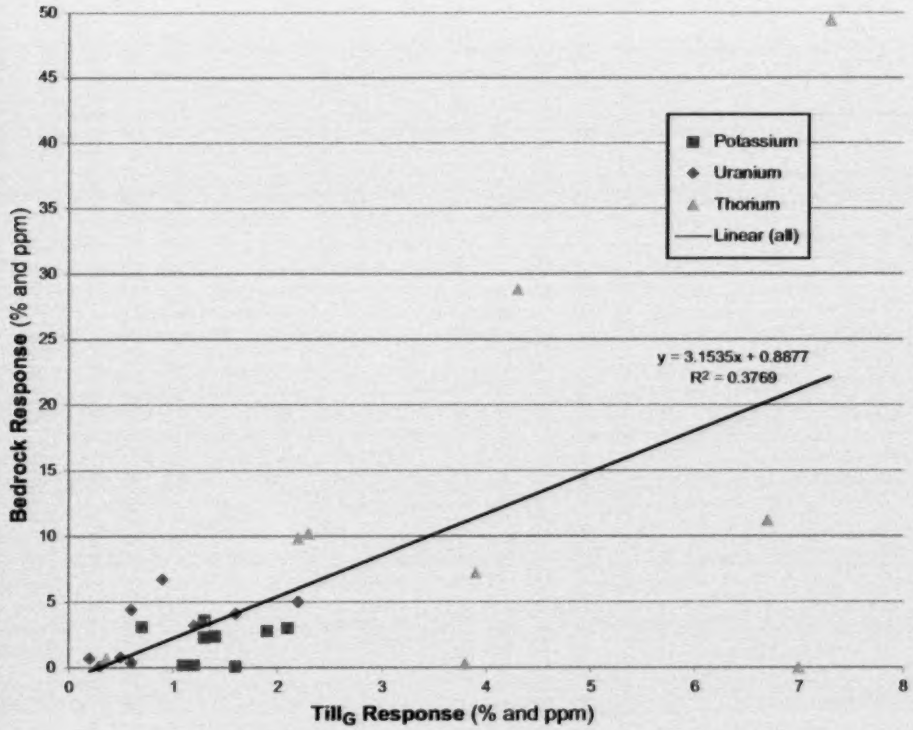

Figure 15. Scatterplot of potassium, equivalent uranium, and equivalent thorium response for bedrock and ground till (Till$_G$) values. The line-of-best-fit incorporates all the data points.

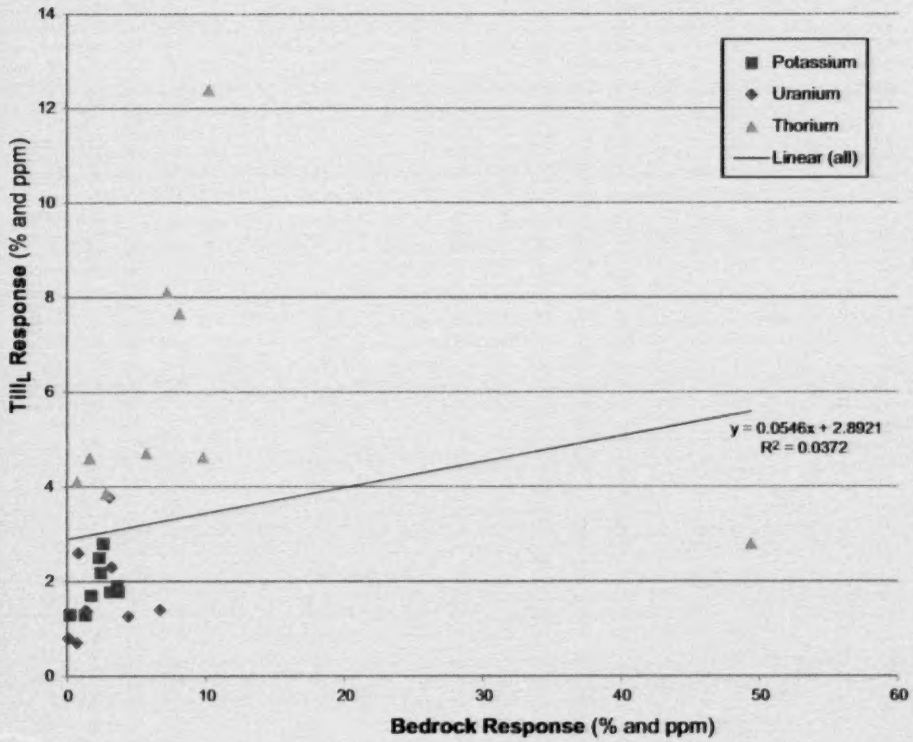

Figure 16. Scatterplot of potassium, equivalent uranium, and equivalent thorium response for bedrock and laboratory measured till (Till$_L$) values. The line-of-best-fit incorporates all the data points.

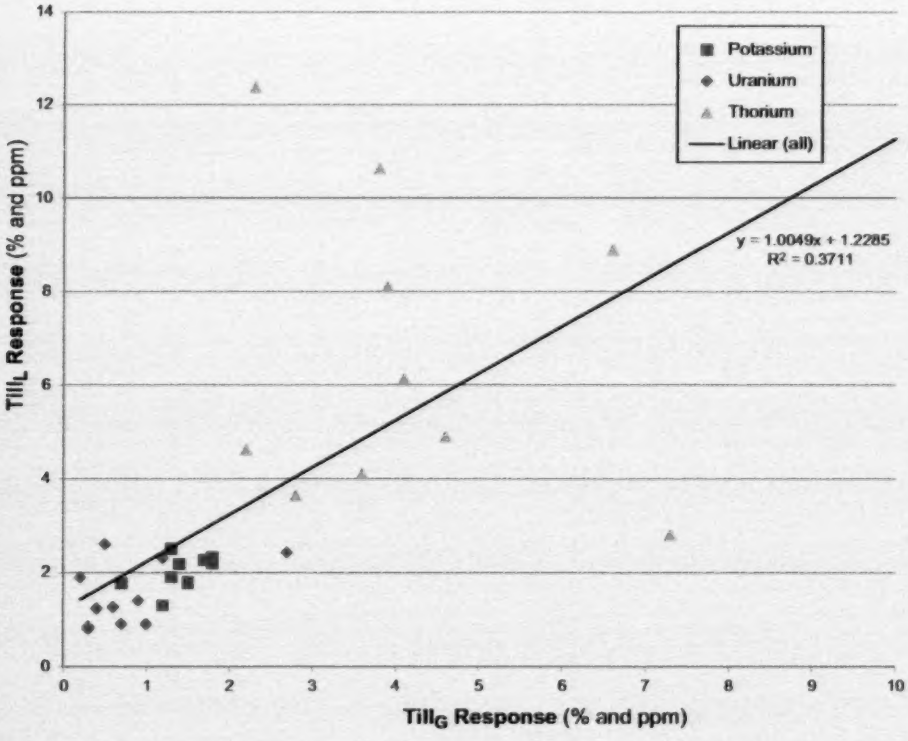

Figure 17. Scatterplot of potassium, equivalent uranium, and equivalent thorium response for till measured in the laboratory ($Till_L$) and on the ground ($Till_G$). The line-of-best-fit incorporates all the data points.

composition to locations with exposed bedrock. Pebble counts for the area support this conclusion and have a high proportion of felsic intrusive lithologies in the till. This would indicate a local till provenance for the majority of the clasts as their composition is similar to local bedrock lithology. Clasts would influence the gamma-ray response because they are contained within and are the parent material of the bulk till a GRS sensor would record. Observations of lower erosive strength due to the migration of the Ancestral Labrador Ice Divide across the De Pas Batholith further enforce the local origin of materials in the eastern portion of the study area (Rice et al., 2016). These results show that the gamma-ray signatures of Domains 2 and 3 are dominated by bedrock sources; these areas have thinner till (Rice et al., 2017) that is locally derived and contains K-feldspar from the De Pas Batholith resulting in a magenta (potassium-dominated) hue on the image (Fig. 11).

The GRS signature of the western domains is dominated by contributions from surface till. The boundaries of these domains are roughly parallel to the regional trends of the underlying bedrock structures. These domains, however, have no alignment with bedrock contacts (Fig. 12) and little bedrock is found at surface (Table 2) (Rice et al., 2017) . Lack of correlation between the airborne radiometric response and the bedrock units is a result of bedrock being covered by more than 0.5 m of till and organics.

Haber et al. (2016) compared the airborne response of many different types of rocks in different scenarios of unconsolidated material thickness. They found an exponential drop in similarity between ground measurements of bedrock and airborne gamma-ray reading as the surface material extent increased beyond a depth of 40 cm. Therefore, in locations where overlying materials are thick, the airborne response is unrelated to bedrock geology. This scenario occurs in the western portion of the study area, where extensive till veneers and till blankets cover the bedrock. The composition of the till therefore influences the delineation of the radiometric domains over the western portion of the study area.

Gamma-ray spectrometry responses that are dominated by the composition of glacially transported sediment have been observed in other glaciated environments (Campbell et al., 2007; Ross et al., 2009; Paulen et al., 2017). In these environments, airborne GRS has been used to differentiate till units, based on potassium, equivalent uranium, and equivalent thorium ratios that reflect the eroded bedrock sources, and to delineate dispersal trains (Fortin et al., 2015; Paulen et al., 2017). Variability in responses over the western portion of the study area can be explained in a similar fashion. The spectral signatures of Domains 5, 7, and 9 show a strong GRS response that is high in equivalent uranium and equivalent thorium (Table 2). As such, these radiometric domains could all be sourced from the same

bedrock unit, indicating a similar provenance, analogous to the findings by Campbell et al. (2007) and Fortin et al. (2015). Pebble counts in the western area show that the majority of the pebbles within this region were sourced from the Laporte Domain metasedimentary rocks, but there is also some mixing of other far-traveled lithologies, such as mafic intrusive clasts.

The orientation of western domains matches the orientation of the lakes and landforms within the region, reflecting glacially streamlining to the northwest (Table 2) (McClenaghan et al., 2016; Rice et al., 2017). The approximate southeast–northwest trend of the domains is similar to that of a dispersal train transported in the major northwest ice-flow direction over this region. Therefore, these domains have a morphology that would suggest a glacial origin for the surficial till.

The influence of the surficial till in delineating the radiometric domains is reinforced by the airborne signal, which correlates best with the ground till readings ($R^2 = 0.78$) (Fig. 14). There are also significant differences between the average in situ bedrock readings and the ground till readings for all radioelements. This indicates that there are two distinct sources in the western part of the study area, and adds support to the till being of regional origin (i.e. inclusion of more distally derived detritus). The combination of the streamlined domains (i.e. Domain 7) with thick till layers and statistical analysis show that the western domains are influenced by surface till.

Airborne GRS differences within these western domains are likely a result of the variable surficial geology. As discussed above, till in Domains 5, 7, and 9 is likely all derived from the same bedrock source. Domains 4 and 5 were likely affected by glaciolacustrine winnowing and washing, creating sandy veneers (<0.5 m) of littoral sediments over the till. Domain 6 corresponds to the upper glaciolacustrine washing limit of glacial Lake McLean, which resulted in boulder lags being deposited on washed bedrock surfaces. Domain 8 is an area with abundant melt-water corridors and veneers of glaciofluvial sediment that is dominated by quartz sand-sized grains overlying the till and bedrock. This could contribute to the whitish and diffuse signal, as quartz does not emit many gamma-rays (Rider, 1990). Furthermore, due to the physiography of the region, Domains 4 and 8 have more water and vegetation, which absorb the gamma-ray response (Grasty et al., 1988; Gastrich et al., 2016). These observations indicate that airborne GRS is useful in semi-quantitatively mapping surficial geology units.

The borders of Domains 11 and 12 do not correspond to bedrock units (Fig. 12) nor do they match any observed surficial geology trend. These two domains are also unique in composition, exhibiting relatively high equivalent uranium content relative to potassium and thorium (Table 1). It is possible that the response is the result of a distinct till deposit originating from a different bedrock source, possibly the Doublet Group metavolcanic rocks that reside to the southwest; the mineral composition and GRS signature of the Doublet Group was not obtained in this study and hence this hypothesis could not be tested.

Comparison of gamma-ray spectrometry datasets

The only datasets that showed a strong correlation were the airborne values and the in situ till readings that were collected at the field sites (Fig. 14, 15, 16, 17). The GRS readings obtained at the bedrock surfaces do not correlate to the airborne survey data because the surface till is attenuating the response coming from the underlying bedrock in most of the domains (Domains 2 and 3 excluded) (Minato, 2002; Haber et al., 2016). Furthermore, some samples that were measured in the laboratory were collected below the active soil horizon at depths of over 0.5 m, which is deeper than airborne and handheld gamma-ray signals can penetrate (International Atomic Energy Agency, 2003). This would imply some disconnect between the readings obtained from surface till and till at depth. With the elimination of the other two GRS datasets, only the surface till layer measured at ground level is correlative to the airborne response across the study area.

Implications for mineral exploration

Several outcomes from this research have implications for mineral exploration in the region. Knowledge of the origin of a domain signal means that anomalies within radiometric domains can be easily investigated by appropriate exploration methods. For example, an airborne GRS anomaly within Domain 2 is indicative of a close mineralized bedrock source since airborne GRS in Domain 2 is most influenced by bedrock geology and till of local provenance. In contrast, an anomaly in Domain 7, where the airborne response is indicative of regionally sourced till that has been moved from its bedrock mineralization, would suggest exploration in the up-ice flow direction. Understanding the source of anomalies can make the exploration process for valuable mineralization more efficient by reducing the area for investigation.

Another implication for mineral exploration is that airborne radiometric readings within the study area are closely related to those of the ground surface till readings (Campbell et al., 2007; Fortin et al., 2015). This is a transferable observation to other areas with airborne GRS coverage and similar glacial histories. Creating a linear regression from the airborne and ground till plots

would provide an empirical estimate for surface till concentrations at a location for a specific airborne GRS value. Radioelement concentrations could then be evaluated in a manner similar to geochemical signals (Boyle, 1988), i.e., through the delineation of dispersal trains to find mineralization of not only uranium and thorium, but also associated minerals such as copper and gold (Ford et al., 2008). This could make the exploration process more effective by differentiating areas with higher and lower potential for mineralization based on their true potassium, equivalent uranium, and equivalent thorium surface response identified from airborne GRS readings.

The research supports the use of airborne GRS methods in identifying areas of interest for mineral exploration. GRS surveys proved effective at differentiating areas of contrasting surface sediments, which can then be linked to the transport history of the sediments and traced back to its source. The close linear relationship between ground and airborne GRS confirms that, when properly processed, airborne data can be good estimates of ground measurements. Though collecting ground in situ measurements can be useful for validation, a ground sampling program can focus on specific targets and anomalous areas, using airborne data as a baseline.

SUMMARY AND CONCLUSIONS

This report summarizes a study to investigate the potential of various gamma-ray data sources as tools for mineral exploration. This was completed by delineating and interpreting radiometric domains and observing possible correlations among in situ bedrock, till measurements taken on the ground, till measurements obtained in the laboratory, and airborne radiometric readings. Twelve radiometric domains, defined as an area of homogenous airborne gamma-ray response (Fortin et al., 2015), were identified. Radiometric domains were further described based on bedrock geology, topography, and surficial geology. Airborne, in situ bedrock, ground till, and laboratory till GRS readings were also integrated and contrasted for analysis within GIS software. When comparing the data sources, only the airborne and ground surface till responses correlated well, resulting in an R^2 value of 0.78 (Fig. 14). All other comparisons showed weaker correlations (Fig. 15, 16, 17). This suggests that for this area of northern Quebec, surface till radio-chemistry is the most discriminating contributor to the gamma-ray signature.

It was established that spectral signatures of radiometric domains located on the eastern side of the study area were related to the bedrock, and that domains on the western side were related to till composition. This is the result of ice-flow dynamics and history, which caused thinner locally sourced till deposits and more extensive bedrock at surface over the eastern portion of the study area. Alternatively, thicker regionally sourced glacial till characterizes the western region, overprinting any bedrock gamma-ray sources. This is further confirmed by the streamlined nature of the domains and the correlation in these areas between airborne and ground till readings. Domains 4 and 8 had weaker responses because of the extent of organics and lakes but the readings still matched the general trends observed for the western side.

It is clear that surficial geology is an important factor when interpreting airborne GRS readings of an area. Specifically, the thickness of the sediments over the bedrock and sediment source (i.e. local, regional, subglacial, glaciolacustrine) are linked to the airborne radioelement concentrations recorded. For example, without knowledge of the extensive till veneers and bedrock outcrop located in the eastern portion of the study area, potassium-rich values could not be readily linked to its bedrock source. Therefore, a detailed knowledge of the surficial geology of an area can significantly improve the interpretations of the radiometric response. Conversely, divergence of the radiometric response can refine the understanding the surficial geology.

Airborne GRS measurements are important as their integration with different gamma-ray sources can aid mineral exploration. The results of this research indicate that, for this particular region, responses from highlands correlate well with bedrock sources, whereas low-lying areas do not. Applying this understanding to radiometric domains means locations of mineralization can be identified more efficiently, reducing the size of the source area to be investigated. Additionally, the link between airborne and ground till GRS methods allows airborne values to be correlated to ground concentrations. Thus potassium, equivalent uranium, and equivalent thorium measurements may be useful for identifying areas of mineral potential.

This preliminary study, which showed a link between airborne GRS and surficial geology for a specific area of Northern Quebec, advances the understanding of the interrelationship of GRS data sources. The research suggests that radiometric domains can be used as a proxy for the composition, provenance, and extent of surficial geology, which may help define areas for mineral exploration.

ACKNOWLEDGEMENTS

This open file constitutes a B.Sc. Honours thesis that was part of the Geological Survey of Canada Geo-Mapping for Energy and Mineral (GEM) 2 Hudson – Ungava Project. The thesis data is based on field and laboratory work completed in conjunction with this

project. Research was completed under the supervision of Professor Emmanuelle Arnaud (University of Guelph, School of Environmental Science), Roger Paulen (Geological Survey of Canada), and Richard Fortin (Geological Survey of Canada). The research benefited from the field assistance of Alain Lion during the 2015 field season, Jessey Rice (University of Waterloo) and Matt Pyne (Geological Survey of Canada) during both the 2015 and 2016 field seasons, and Heather Campbell (Newfoundland and Labrador Geological Survey) for the 2016 field season. Additionally, Alain Rioux and Maxime Gauthier of Innukopters Inc. provided helicopter service, Clara Schattler and Gestion Porlier provided accommodation and meals, and Norpaq Aviation provided expediting services. This logistical support is greatly appreciated. Janet Campbell is also thanked for her diligent review of this document.

REFERENCES

Barnett, D., 1967. Glacial Lake MacLean and its relationship with Glacial Lake Naskaupi; Geographical Bulletin, v. 9, no. 96, p. 101.

Beamish, D., 2016. Enhancing the resolution of airborne gamma-ray data using horizontal gradients; Journal of Applied Geophysics, v. 132, p. 75–86.

Bostock, H., 1970. Physiographic regions of Canada; Geological Survey of Canada, Map 1254A, scale 1:5,000,000.

Boyle, D., 1988. Airborne radiometrics and U-Th-K-Sn lithogeochemistry in prospecting for tin deposits in the Davis Lake pluton, southwestern Nova Scotia, *In:* Prospecting in Areas of Glaciated Terrain 1988, (ed.) D.R. MacDonald; Canadian Institute of Mining and Metallurgy, p. 599–624.

Broome, J., Carson, J., Grant, J., and Ford, K., 1987. A Modified Ternary Radioelement Mapping Technique and Its Application to the South Coast of Newfoundland; Geological Survey of Canada, Paper 87–14.

Campbell, J., Klassen, R., and Shives, R., 2007. Integrated field investigations of airborne radiometric data and drift composition, Nuclear Energy Agency–International Atomic Energy Agency Athabasca test area, Saskatchewan, *In:* EXTECH IV: Geology and Uranium Exploration Technology of the Proterozoic Athabasca Basin, Saskatchewan and Alberta, (ed.) C. Jefferson and G. Delaney; Geological Survey of Canada, Bulletin 588, p. 533–554.

Canadian Centre for Mapping and Earth Observation., 1997. Canadian Digital Elevation Data 23P Lac Resolution; Government of Canada.

Corrigan, D., Pehrsson, S., Wodicka, N., and de Kemp, E., 2009. The Paleoproterozoic Trans-Hudson Orogen: a prototype of modern accretionary processes, *In:* Ancient Orogens and Modern Analogues, J.B. Murphy, J.D. Keppie, and A.J. Hynes; Geological Society, London, Special Publications, v. 327, p. 457–479.

D'Amours, I. and Intissar, R., 2013. Magnetic and airborne spectrometric survey in the Romanet Lake area, Churchill Province; Natural Resources Québec, Summary Report. p.8

Ford, K., Harris, J. R., Shives, R., Carson, J., and Buckle, J., 2008. Remote predictive mapping 2. Gamma-ray spectrometry: a tool for mapping Canada's north; Geoscience Canada, v. 35, no. 3-4, p. 109–126.

Fortin, R., Campbell, J., Harvey, B., McCurdy, M., Sinclair, L., Hanson, M., Potter, E., and Jefferson, C., 2015. Ground-truthing of the 'Eastern Athabasca Basin' regional airborne gamma-ray survey: context for exploration of deeply buried unconformity-related uranium deposits in the Athabasca Basin of northern Saskatchewan, *In:* Targeted Geoscience Initiative 4: Unconformity-related Uranium Systems, (ed.) E.G. Potter and D.M. Wright; Geological Survey of Canada, Open File 7791, p. 43–51.

Gastrich, H., Göbling, C., Klingenberg, R., Kröninger, K., Neddermann, T., Nitsch, C., and Zuber, K., 2016. The dortmund low background facility—low-background gamma ray spectrometry with an artificial overburden; Applied Radiation and Isotopes, v. 112, p. 165–176.

Grasty, R., Wilkes, P., and Kooyman, R., 1988. Background Measurements in Gamma-ray Surveys; Geological Survey of Canada. Paper 88-11, p. 40.

Guastaldi, E., Baldoncini, M., Bezzon, G., Broggini, C., Buso, G., Caciolli, A., Carmignani, L., Callegari, I., Colonna, T., Dule, K., and Fiorentini, G., 2013. A multivariate spatial interpolation of airborne γ-ray data using the geological constraints; Remote Sensing of Environment, v. 137, p. 1–11.

Haber, D., Malchow, R., and Burnley, P., 2016. Monte Carlo simulations of the gamma-ray exposure rates of common rocks; Journal of Environmental Radioactivity, v. 167, p. 20–25.

International Atomic Energy Agency., 2003. Guidelines for Radioelement Mapping using Gamma Ray Spectrometry Data; International Atomic Energy Agency, Technical Reports Series No. 1363. p. 179.

International Atomic Energy Agency., 1987. Preparation and Certification of IAEA Gamma-ray Spectrometry Reference Materials RGU-1, RGTh-1 and RGK-1; International Atomic Energy Agency, Technical Reports IAEA/RL/148, 48 p.

Ives, J., 1960. Former ice-dammed lakes and the deglaciation of the middle reaches of the George River, Labrador-Ungava; Geographical Bulletin, v. 14, p. 44–70.

Jansson, K., 2003. Early Holocene glacial lakes and ice marginal retreat pattern in Labrador/Ungava, Canada; Palaeogeography, Palaeoclimatology, Palaeoecology, v. 193, no. 3, p. 473–501.

Jansson, K., Stroeven, A., and Kleman, J., 2003. Configuration and timing of Ungava Bay ice streams, Labrador-Ungava, Canada; Boreas, v. 32, p. 256–262.

Kearey, P., Brooks, M., and Hill, I., 2013. An Introduction to Geophysical Exploration; John Wiley & Sons. p. 281.

Klassen, R. and Thompson, F., 1993. Glacial History, Drift Composition, and Mineral Exploration, central Labrador; Geological Survey of Canada, Bulletin 435.

McClenaghan, M., Paulen, R., Rice, J., McCurdy, M., Amor, S., Garrett, R., Solgadi, F., Fortin, R., Spirito, W., Adcock, S., Ross, M., Campbell, H., Pyne, M., and Hagedorn, G., 2016. GEM 2 Hudson- Ungava project 2016 Report of Activities for the Core Zone: Surficial Geology, Geochemistry, and Gamma-ray Spectrometry Studies in northern Quebec and Labrador; Open File 8148, 23 p. doi:10.4095/299295

McClenaghan, M., Plouffe, A., McMartin, I., Campbell, J., Spirito, W., Paulen, R., Garrett, R., and Hall, G., 2013. Till sampling and geochemical analytical protocols used by the Geological Survey of Canada; Geochemistry: Exploration, Environment, Analysis, v. 13, no. 4, p. 285–301.

Minato, S., 2002. Simple soil mass balance approach to interpret the distribution of global terrestrial gamma ray dose rates in relation to geology; Science of the Total Environment, v. 298, no. 1, p. 229–231.

Ministère de l'Énergie et des Ressources naturelles., 2010. CG SIGEOMM23P, SIGEOM Geological Maps for sheet 23P, 16 maps, scale 1:50 000.

Minty, B., 1997. Fundamentals of airborne gamma-ray spectrometry; Australian Geological Survey Organisation, Journal of Australian Geology and Geophysics, v. 17, p. 39–50.

Paulen, R., Stokes, C., Fortin, R., Rice, J., Dubé-Loubert, H., and McClenaghan, M., 2017. Dispersal trains produced by ice streams: An example from Strange Lake, Labrador, Canada, *In:* Proceedings of the Sixth Decennial International Conference on Mineral Exploration, 2017.

Radiation Solutions Incorporated., 2016. RS-230 BGO Super Spec Handheld Gamma-Ray Spectrometer Manual; Radiation Solutions Incorporated.

Rice, J., Paulen, R., Campbell, H., Ross, M., Pyne, M., and Hagedorn, G., 2016. Surficial mapping, Chapter 2 *In:* Report of Activities for the Core Zone: 2016 Surficial Geology, Geochemistry, and Gamma-ray Spectrometry Studies in northern Quebec and Labrador, (ed.) McClenaghan and 13 others; Geological Survey of Canada, Open File 8148, p. 11–18.

Rice, J., Paulen, R., Ross, M., 2017. Surficial geology, De Pas River, Quebec, NTS 23-P northwest; Geological Survey of Canada, Canadian Geoscience Map 317, (preliminary edition) 1 sheet. Scale 1:100 000.

Rider, M., 1990. Gamma-ray log shape used as a facies indicator: critical analysis of an oversimplified methodology; Geological Society, London, Special Publications, v. 48, no. 1, p. 27–37.

Ross, M., Campbell, J., Parent, M., and Adams, R., 2009. Palaeo-ice streams and the subglacial landscape mosaic of the North American mid-continental prairies; Boreas, v. 38, p. 421–439.

Sanborn-Barrie, M., 2016. Refining lithological and structural understanding of the southern Core Zone, northern Quebec and Labrador in support of mineral resource assessment; Geological Survey of Canada, Open File 7965, 39 p. doi:10.4095/297560

Spirito, W., McClenaghan, M., Plouffe, A., McMartin, I., Campbell, J., Paulen, R., Garret, R., and Hall, G., 2011. Till sampling and analytical protocols for GEM Projects: from field to archive; Geological Survey of Canada, Open File 6850. 83 p. doi:10.4095/288752

Veillette, J., Dyke, A., Roy, M., 1999. Ice-flow evolution of the Labrador sector of the Laurentide Ice Sheet: A review, with new evidence from northern Quebec; Quaternary Science Reviews, v. 18, no. 8-9, p. 993–1019.

Vincent, J., 1989. Quaternary geology of the southeastern Canadian Shield, Chapter 3 *In:* Quaternary Geology of Canada and Greenland, (ed.) R.J. Fulton; Geological Survey of Canada, Geology of Canada Series No. 1, p. 249–275.

Wardle, R. and Bailey, D., 1981. Early Proterozoic sequences in Labrador, *In:* Proterozoic Basins in Canada, (ed.) F.H.A. Campbell; Geological Survey of Canada, Special Paper 81-10, p. 331–359.

Youssef, M., 2016. Relationships between ground and airborne gamma-ray spectrometric survey data, North Ras Millan, Southern Sinai Peninsula, Egypt; Journal of Environmental Radioactivity, v. 152, p. 75–84.

Youssef, M. and Elkhodary, S., 2013. Utilization of airborne gamma ray spectrometric data for geological mapping, radioactive mineral exploration and environmental monitoring of southeastern Aswan city, South Eastern Desert, Egypt; Geophysical Journal International, v. 195, no. 3, p. 1689–1700.

APPENDICES

Appendix A1. Site location information and results of field gamma-ray spectrometer measurements.

Easting (m)	Northing (m)	Elevation (m ASL)	Sample number	Total (ppm)	Total (cpm)	K (%)	K (cpm)	U (ppm)	U (cpm)	Th (ppm)	Th (cpm)	Dose (Gy/h)	Material
325768	6180672	585	15-PTA-004	343.6	1326.5	1.2	252.5	0.2	10.5	3.1	26.8	25.9	till
325768	6180672	585	15-PTA-004	319.6	1233.9	1.0	210.8	0.3	13.7	4.0	34.1	25.4	till
325641	6180670	585	15-PTA-004	80.4	310.2	0.2	48.8	0.0	0.1	0.6	4.8	4.8	bedrock
325641	6180670	585	15-PTA-004	78.2	301.9	0.2	37.3	0.2	5.3	0.7	5.9	5.2	bedrock
315731	6188474	485	15-PTA-005	413.4	1596.0	1.7	342.5	0.2	11.6	3.8	32.0	33.6	till
331433	6186567	520	15-PTA-012	2429	9375.3	3.6	946.3	6.7	231.2	49.4	431.3	216.5	bedrock
331433	6186567	520	15-PTA-012	521.8	2014.4	1.3	280.9	0.9	32.5	7.3	63.4	41.3	till
333385	6171351	648	15-PTA-013	422.3	1630.3	1.5	315.3	1.0	26.2	4.1	35.2	36.1	till
324406	6164557	492	15-PTA-018	417.2	1610.7	1.3	280.9	1.2	29.4	3.9	34.1	34.3	till
324330	6164720	492	15-PTA-018	837.9	3234.9	2.3	507.1	3.2	71.2	7.2	63.4	67.0	bedrock
315577	6168428	512	15-PTA-019	989.7	3820.8	3.1	682.9	4.3	92.2	8.4	73.9	86.7	bedrock
315606	6168359	512	15-PTA-019	665.2	2568.2	2.1	460.7	1.8	48.2	7.8	67.6	58.7	bedrock
318892	6179379	494	15-PTA-020	419.4	1619.1	1.5	317.4	0.4	14.7	4.1	35.2	33.3	till
329153	6191473	524	15-PTA-021	1294	4995.9	0.2	82.6	4.1	70.3	0.0	2.8	24.4	bedrock
329037	6191489	524	15-PTA-021	535.0	2065.5	1.2	268.4	1.6	42.9	7.0	61.3	42.7	till
341337	6183674	519	15-PTA-022	253.5	978.8	0.7	154.3	0.6	14.7	2.2	19.5	18.6	till
341337	6183674	519	15-PTA-022	1056	4075.0	3.1	679.7	4.4	97.4	9.8	86.5	90.5	bedrock
322992	6185430	571	15-PTA-082	430.8	1662.9	1.6	320.6	0.2	11.6	3.8	32.0	32.0	till
322931	6185440	571	15-PTA-082	71.2	274.8	0.1	37.3	0.7	12.6	0.3	2.8	6.4	bedrock
329245	6184061	509	15-PTA-083	319.2	1232.3	1.3	272.3	1.3	27.2	2.8	24.7	31.1	bedrock
350549	6152905	583	15-PTA-140	821.5	3171.3	3.5	708.6	0.4	14.7	5.0	41.4	61.8	
350549	6152905	583	15-PTA-140	836	3227.4	3.7	745.3	1.4	33.6	5.7	48.8	70.7	bedrock
313832	6200499	473	15-PTA-163	544.7	2102.9	1.3	296.5	1.9	48.2	6.8	59.2	45.5	bedrock
315447	6191119	512	15-PTA-164	319.9	1235.0	1.1	231.7	0.9	23.1	3.6	31.0	28.6	till
316507	6173505	517	15-PTA-002	648.9	2505.1	1.8	408.5	2.7	60.7	6.6	58.2	56.3	till
337598	6155234	593	15-PTA-165	493	1903.3	2.1	428.2	1.0	25.2	4.0	34.1	43.4	bedrock
338538	6205647	483	15-PTA-010	686.3	2649.4	2.4	513.9	0.8	35.6	10.2	87.4	63.4	bedrock
338540	6205639	483	15-PTA-010	389.9	1505.2	1.4	277.7	0.5	12.6	2.3	19.5	26.7	till
354106	6198160	615	15-PTA-011	490.9	1895.0	1.8	380.1	0.7	22.0	4.6	39.3	40.4	till
364869	6179124	569	15-PTA-024	357.8	1381.2	1.7	349.7	0.7	13.7	1.6	13.2	30.6	bedrock
354958	6173645	585	15-PTA-029	361.4	1395.2	1.5	306.9	0.3	10.5	2.8	23.7	29.0	till
356331	6154903	571	15-PTA-159	552.0	2131.1	2.3	465.8	0.8	20.0	3.9	33.1	44.5	bedrock
361037	6162096	610	15-PTA-160	377.6	1457.9	1.5	299.6	0.1	9.5	3.7	31.0	29.8	bedrock
330693	6194771	509	16-PTA-053	1099.0	4330.8	3.5	736.5	2.0	66.3	13.7	118.9	93.5	bedrock
345428	6182862	491	16-PTA-063	1353.0	5331.2	2.8	639.3	0.4	78.7	28.8	249.4	117	bedrock
345441	6182873	494	16-PTA-063	473.6	1865.9	1.9	375.7	0.6	19.4	4.3	37.4	39.0	till
345099	6173909	552	16-PTA-064	1124	4427.6	3.0	671.1	5.0	110.8	11.2	99.6	96.9	bedrock
345132	6173852	548	16-PTA-064	692.7	2729.4	2.1	447.5	2.2	52.0	6.7	58.5	57.1	till
340641	6169687	497	16-PTA-065	489.3	1927.7	2.4	474.1	0.5	11.0	1.3	11.0	38.2	bedrock
322153	6170597	518	16-PTA-071	487.5	1920.7	1.6	337.9	1.5	34.0	4.0	34.9	39.8	till
339891	6179597	524	16-PTA-072	466.3	1837.3	1.7	343.5	0.5	18.7	4.4	37.8	36.7	till
331401	6191560	487	16-PTA-073	1472.0	5798.9	2.9	678.5	3.7	120.0	23.4	204.5	121.6	till
332859	6197952	465	16-PTA-074	438.2	1726.3	1.6	317.2	0.7	21.0	3.9	33.6	34.6	till
325988	6190098	513	16-PTA-075	976.9	3848.8	3.9	798.6	2.5	53.7	5.6	49.3	80.1	bedrock
325988	6190098	513	16-PTA-075	996.2	3925.0	4.2	851.4	2.7	58.5	5.9	52.1	85.6	bedrock
336075	6163894	538	16-PTA-147	97.8	385.4	0.3	57.3	0.2	4.5	0.7	6.2	6.5	bedrock
321132	6171488	466	16-PTA-149	2608.0	10274.1	4.1	1031.3	10.6	277.1	40.5	357.2	219.8	bedrock
321132	6171480	466	16-PTA-149	2209.0	8702.8	3.8	916.5	6.0	197.6	39.4	344.4	187.8	bedrock

Appendix A2. Site location information and results of laboratory gamma-ray spectrometer measurements.

Sample number	Easting (m)	Northing (m)	K (%)	U (ppm)	Th (ppm)	Weight (grams)	Date	Note
16-PTA-056	312003	6175876	2.30	2.62	6.60	467.83	1/23/2017	
16-PTA-069	360714	6177273	1.79	0.78	4.00	554.79	1/23/2017	
16-PTA-069	360714	6177273	1.78	0.52	4.73	554.80	1/31/2017	
16-PTA-070	358871	6184278	1.70	0.78	4.06	514.76	1/23/2017	
16-PTA-070	358871	6184278	1.69	0.33	4.68	514.72	1/31/2017	
15-PTA-002	316747	6173641	2.18	2.83	9.23	295.91	7/20/2016	<2 mm
15-PTA-002	316747	6173641	2.33	2.19	8.15	396.70	6/20/2016	<2 mm
15-PTA-002	316747	6173641	2.38	3.02	8.43	438.53	6/3/2016	bulk
15-PTA-002	316747	6173641	2.40	1.65	9.75	492.20	5/27/2016	bulk
15-PTA-003	316122	6157626	1.80	2.00	5.10	394.13	7/26/2016	<2 mm
15-PTA-003	316122	6157626	1.76	2.44	4.78	384.23	6/3/2016	bulk
15-PTA-004	325774	6180779	1.23	1.03	4.00	373.99	7/26/2016	<2 mm
15-PTA-004	325774	6180779	1.36	0.55	4.19	420.21	6/8/2016	bulk
15-PTA-005	315734	6188471	1.40	1.03	5.05	335.02	7/26/2016	<2 mm
15-PTA-005	315734	6188471	2.84	2.61	17.21	356.62	6/16/2016	<2 mm
15-PTA-005	315734	6188471	1.45	1.30	5.03	322.34	6/3/2016	bulk
15-PTA-005	315734	6188471	3.38	2.64	15.26	527.56	5/24/2016	bulk
15-PTA-007	314247	6201443	1.87	1.44	7.19	437.57	7/26/2016	<2 mm
15-PTA-007	314247	6201443	2.75	4.02	20.48	324.21	6/20/2016	<2 mm
15-PTA-007	314247	6201443	1.93	1.48	6.31	459.96	6/3/2016	bulk
15-PTA-007	314247	6201443	3.59	3.71	17.90	540.22	5/24/2016	bulk
15-PTA-008	324146	6196548	2.60	3.60	18.23	377.32	7/11/2016	<2 mm
15-PTA-008	324146	6196548	1.79	1.04	5.91	378.19	6/15/2016	<2 mm
15-PTA-008	324146	6196548	2.02	1.01	5.72	410.82	6/8/2016	bulk
15-PTA-008	324146	6196548	2.72	4.01	19.53	529.18	5/27/2016	bulk
15-PTA-009	329892	6195997	2.18	1.98	9.71	327.00	7/11/2016	<2 mm
15-PTA-009	329892	6195997	2.47	1.95	11.54	523.34	5/27/2016	bulk
15-PTA-010	338541	6205625	2.36	4.29	19.97	373.01	6/16/2016	<2 mm
15-PTA-010	338541	6205625	2.01	0.85	4.53	369.43	6/15/2016	<2 mm
15-PTA-010	338541	6205625	1.91	1.47	4.79	342.64	6/6/2016	bulk
15-PTA-010	338541	6205625	2.45	3.80	20.25	523.00	5/24/2016	bulk
15-PTA-011	354109	6198158	2.08	0.74	4.72	411.41	6/16/2016	<2 mm
15-PTA-011	354109	6198158	2.18	0.96	5.04	415.48	6/3/2016	bulk
15-PTA-012	331398	6186586	1.78	1.38	5.44	398.50	6/16/2016	<2 mm
15-PTA-012	331398	6186586	1.85	1.32	6.15	465.43	6/6/2016	bulk
15-PTA-013	333808	6171313	1.72	0.87	5.73	348.90	6/16/2016	<2 mm
15-PTA-013	333808	6171313	1.85	0.87	6.45	335.45	6/8/2016	bulk
15-PTA-014	329539	6163488	1.75	1.23	4.97	344.34	6/11/2016	<2 mm
15-PTA-014	329539	6163488	1.84	1.39	6.00	421.43	6/6/2016	bulk
15-PTA-018	324300	6164569	2.40	2.37	7.32	334.59	6/11/2016	<2 mm
15-PTA-018	324300	6164569	2.54	2.08	8.79	429.21	6/8/2016	bulk
15-PTA-019	315607	6168353	2.96	3.61	7.33	286.10	6/11/2016	<2 mm
15-PTA-019	315607	6168353	2.63	3.92	7.98	185.21	5/31/2016	bulk
15-PTA-020	318911	6179366	1.73	1.41	6.05	407.80	6/15/2016	<2 mm
15-PTA-020	318911	6179366	1.82	1.05	6.22	466.88	6/6/2016	bulk
15-PTA-022	341310	6183672	1.61	1.37	4.00	432.62	6/11/2016	<2 mm
15-PTA-022	341310	6183672	1.94	1.15	5.25	487.93	6/8/2016	bulk
15-PTA-024	364858	6179133	1.72	0.67	4.64	411.54	6/11/2016	<2 mm
15-PTA-024	364858	6179133	1.67	0.72	4.51	463.39	6/7/2016	bulk
15-PTA-025	325027	6171115	2.04	1.33	5.56	398.97	6/11/2016	<2 mm
15-PTA-026	325423	6159190	2.09	1.02	5.62	492.43	6/1/2016	bulk
15-PTA-028	338498	6159358	3.15	2.11	10.57	368.77	6/15/2016	<2 mm
15-PTA-028	338498	6159358	2.22	0.55	3.56	484.92	6/1/2016	bulk
15-PTA-029	354958	6173645	1.77	1.01	3.39	370.30	6/11/2016	<2 mm
15-PTA-029	354958	6173645	1.83	0.67	3.89	523.52	6/1/2016	bulk
15-PTA-034	370875	6190479	2.06	0.94	4.94	404.60	6/15/2016	<2 mm
15-PTA-034	370875	6190479	2.22	0.45	5.66	376.01	5/31/2016	bulk
15-PTA-036	359584	6206610	2.08	0.80	4.53	366.95	6/11/2016	<2 mm
15-PTA-036	359584	6206610	2.33	0.41	5.65	384.14	6/1/2016	bulk

Appendix A2 continued.

Sample number	Easting (m)	Northing (m)	K (%)	U (ppm)	Th (ppm)	Weight (grams)	Date	Note
15-PTA-037	376131	6203836	1.95	1.24	5.03	410.02	7/26/2016	<2 mm
15-PTA-037	376131	6203836	2.23	1.28	6.08	395.94	6/1/2016	bulk
15-PTA-043	363192	6167321	1.74	0.79	5.19	373.12	7/26/2016	<2 mm
15-PTA-043	363192	6167321	1.77	0.89	4.50	320.49	5/31/2016	bulk
15-PTA-056	339088	6189004	1.77	1.01	4.36	439.81	6/16/2016	<2 mm
15-PTA-056	339088	6189004	1.98	0.94	4.62	559.79	6/7/2016	bulk
15-PTA-057	325639	6190090	1.77	1.37	6.45	365.35	6/15/2016	<2 mm
15-PTA-057	325639	6190090	1.86	1.30	5.71	479.73	6/6/2016	bulk
15-PTA-083-C	329287	6184065	1.23	0.66	4.02	420.34	7/11/2016	<2 mm
15-PTA-083-C	329287	6184065	1.35	0.58	3.68	417.57	5/26/2016	bulk
15-PTA-098	349742	6187989	1.78	0.77	3.97	460.06	6/11/2016	<2 mm
15-PTA-098	349742	6187989	2.03	0.55	4.61	537.44	5/26/2016	bulk
15-PTA-099	369396	6183594	1.98	1.88	5.48	381.02	6/15/2016	<2 mm
15-PTA-099	369396	6183594	2.22	2.02	5.73	454.03	6/3/2016	bulk
15-PTA-139	365162	6159047	1.85	1.56	5.42	357.22	7/26/2016	<2 mm
15-PTA-139	365162	6159047	1.80	1.40	6.07	401.59	5/24/2016	bulk
15-PTA-140	350472	6152900	1.78	1.32	4.10	251.24	7/19/2016	<2 mm
15-PTA-140	350472	6152900	1.78	1.42	5.31	416.04	6/3/2016	bulk